Chapter 16

Basic ART Resonators

§ 1. Natural and Artificial ART

For the most part, when one reads or hears of an ART network, the network being discussed is an artificial neural network machine. Indeed, the first two widely disseminated papers in which the term "ART network" was used were published in *Computer, Vision, Graphics, and Image Processing* [CARP2] and in *Applied Optics* [CARP3]. As one might expect from these titles, the systems there described are machines intended for specific engineering applications, and I believe it is not unfair to say their connection to biological signal processing is latent and lies hidden in the shade of some of the references cited in these works. To use the time-worn phrase favored by artificial neural network theorists, ART1 and ART2 are "inspired by biology." This is to say that unless one believes biological neural networks exist that do such things as calculate L_2 norms (more commonly known as Euclidean distance), the artificial networks should not be held to be representations of natural neural networks, but at best merely approximations of neural function.

This is in no way meant to denigrate the artificial ART networks of the engineering and mathematical worlds. Quite the contrary. They are powerful and useful machines for carrying out various engineering signal processing tasks. Nor does this imply that these artificial networks carry *no* connection with biological signal processing. The artificial ART networks of the 1980s and 1990s owe their foundation to the 1970s work carried out by Grossberg in modeling neurological and psychological phenomena. But it is to say that they are fundamentally *algorithms* and the tasks they carry out are mathematico-engineering tasks. Many practitioners of artificial neural network theory are fond of implying that this field of engineering and mathematics is a manifestation of the same sort of underlying principles that govern the function of the brain, and perhaps to some degree this is true. But at the present time to make such an implication on behalf of *any* artificial neural network structure is to engage in romantic speculation rather than natural science.

Still, as was just noted, the *design strategy* for ART1, ART2, ART3, ARTMAP, etc. does draw from work that was aimed at understanding biological systems, and from mathematical consequences that appear to follow from empirical findings in psychology and neurology. Our pedagogical objective in this chapter is to introduce and understand what some of these consequences are. We shall concern ourselves with adaptive resonance theory and its structures insofar as they have relevance for biological signal processing on the very large scale and for computational neuroscience in general. In the process of coming to this understanding, the reader will also acquire the background needed to appreciate the types of approximations and simplifications engineers make in constructing artificial ART systems, and perhaps even to develop an eye for spotting the points where artificial ART systems employ mathematical structures for which there is no presently known biological foundation.

What is the objective of an artificial ART network design? Carpenter and Grossberg describe this quite succinctly:

> Adaptive resonance architectures are neural networks that self-organize stable pattern recognition codes in real-time in response to arbitrary sequences of input patterns. This article introduces ART 2, a class of adaptive resonance architectures which rapidly self-organize pattern recognition categories in response to arbitrary sequences of either analog or binary input patterns. In order to cope with arbitrary sequences of analog input patterns, ART 2 architectures embody solutions to a number of design principles, such as the stability-plasticity tradeoff, the search-direct access tradeoff, and the match-reset tradeoff. In these architectures, top-down learned expectation and matching mechanisms are critical in self-stabilizing the code learning process. A parallel search scheme updates itself adaptively as the learning process unfolds, and realizes a form of real-time hypothesis discovery, testing, learning, and recognition. After learning self-stabilizes, the search process is automatically disengaged. Thereafter input patterns directly access their recognition codes without any search. Thus recognition time for familiar inputs does not increase with the complexity of the learned code. A novel input pattern can directly access a category if it shares invariant properties with the set of familiar exemplars of that category. A parameter called the attentional vigilance parameter determines how fine the categories will be. If vigilance increases (decreases) due to environmental feedback, then the system automatically searches for and learns finer (coarser) recognition categories. Gain control parameters enable the architecture to suppress noise up to a prescribed level. The architecture's global design enables it to learn effectively despite the high degree of nonlinearity of such mechanisms [CARP3].

Most of the properties and abilities cited here for ART2 are also directly relevant for natural neural network systems. We will see the requirement for these functional abilities arise as a quite natural part of the ART dynamics presented in this chapter. We will not, however, make any attempt to present a general "class of adaptive resonance architectures." To present a "class" is to present in the abstract, and it is a psychological fact that people do not learn from the abstract to the particular but, rather, from the reverse. It is one thing to present in the abstract in an archival journal – as most papers on ART do – and something else to present the ideas of a theory in a textbook. Therefore, here we will develop adaptive resonance theory through examples, from which we will be able to discern the origin of and the need for solutions to such things as "the stability-plasticity tradeoff, the search-direct access tradeoff, and the match-reset tradeoff" of which Carpenter and Grossberg speak in the quote just given. We will see the need for such solutions arising as consequences of specific signal processing issues and limitations of particular subsystems within the ART framework.

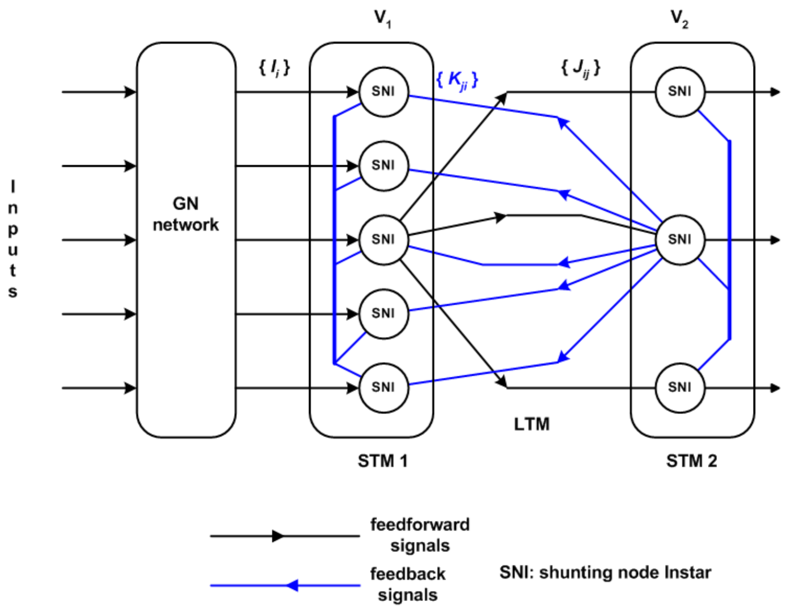

Figure 16.1: The Resonator 1 subsystem. The Grossberg normalizer layer is optional but for purposes of discussion it will be assumed to be a GN$^{(2)}$ anatomy. Layers v_1 and v_2 are competitive layers. The shunting node Instars in v_1 are type SNI$^{(3)}$. In layer v_2 the nodes are comprised of pairs of SNI$^{(3)}$ Instars and Outstars as depicted in figure 14.3. STM denotes short term memory. LTM denotes long term memory. LTM is comprised of a set of feedforward weights **W** from v_1 to v_2 and a set of feedback weights **Z** from v_2 to v_1. The GN and v_1 layers have n nodes, and the v_2 layer has N nodes. I_i, J_{ij}, and K_{ji} are signals.

§ 2. Resonator 1

The heart of an ART network is a subsystem called the ***adaptive resonator***. There are a number of versions of adaptive resonators. Figure 16.1 illustrates the prototype upon which most others are based, either as specializations of it or enhancements of it. We will call this anatomy ***resonator 1*** or R$^{(1)}$ for short. We have already encountered all the pieces that go into its makeup in the previous chapters, especially chapter 15. It consists of three layers. Layer 0 is a Grossberg normalizer, which we will here assume to be GN$^{(2)}$. This layer is actually optional, and if the resonator is driven by the Instar outputs of another resonator GN can be omitted. The GN layer is in some ways a redundancy since the signal normalization function it performs can be handled by layer v_1. Layer 1 (v_1) is a competitive contrast enhancer, specifically the CE used in classifier CL$^{(2)}$ in chapter 15. We will hereafter refer to this as CE$^{(2)}$. Both GN and v_1 have n nodes. Layer 2 (v_2) is also a competitive contrast enhancer with SNI nodes comprising a second CE$^{(2)}$ network. However, in addition each SNI$^{(3)}$ node in v_2 also drives an Outstar node, which is the source of the feedback from v_2 to v_1. Layer v_2 contains N nodes.

Each SNI in v_1 receives a forward-path input signal I_i from its corresponding node in the GN and a set of N feedback signals K_{ji} from v_2. These are summed to produce its total input signal ξ_i. Each SNI in v_2 receives a set of n feedforward signals J_{ij} from each SNI in v_1, which are summed to produce its total input signal ξ_j. In vector-matrix form we have

$$\begin{bmatrix}\xi_1\\ \xi_2\\ \vdots\\ \xi_n\end{bmatrix} = \begin{bmatrix}I_1\\ I_2\\ \vdots\\ I_n\end{bmatrix} + \gamma\cdot\begin{bmatrix}z_{11}\ z_{21}\cdots z_{N1}\\ z_{12}\ z_{22}\cdots z_{N2}\\ \vdots\\ z_{1n}\ z_{2n}\cdots z_{Nn}\end{bmatrix}\cdot\begin{bmatrix}h_2(x_{21})\\ h_2(x_{22})\\ \vdots\\ h_2(x_{2N})\end{bmatrix} \quad \text{or} \quad \boldsymbol{\xi}_1 = \mathbf{I}_1 + \gamma\cdot\mathbf{Z}\cdot h_2(\mathbf{x}_2). \qquad (16.1)$$

Here γ is a constant we will call the ***feedback gain*** and $h_2(u)$ is an activation function for the v_2 SNI excitation variables x_{2j}. **Z** is the matrix of Outstar weights. The second term on the right-hand side of (16.1) defines the K_{ji} variables. As for the J_{ij} inputs to v_2, these are given by

$$\begin{bmatrix}\xi_1\\ \xi_2\\ \vdots\\ \xi_N\end{bmatrix} = \begin{bmatrix}w_{11}\ w_{21}\cdots w_{n1}\\ w_{12}\ w_{22}\cdots w_{n2}\\ \vdots\\ w_{1N}\ w_{2N}\cdots w_{nN}\end{bmatrix}\cdot\begin{bmatrix}x_{11}\\ x_{12}\\ \vdots\\ x_{1n}\end{bmatrix} \quad \text{or} \quad \boldsymbol{\xi}_2 = \mathbf{W}\cdot\mathbf{x}_1. \qquad (16.2)$$

where **W** is the matrix of feedforward weights. For convenience we will abbreviate the columns of the **Z** matrix as Z_i and the rows of the **W** matrix as W_j^T.

Each Instar node in v_1 and v_2 is governed by the dynamical equation (14.31) for SNI$^{(3)}$ and simulated using the difference equation form (14.33). As we did in chapter 15, we will impose the constraint that all x_{1i} and x_{2j} variables must remain non-negative (i.e., we will clip them at zero if the equation would take them less than zero). As noted in chapter 15, this is equivalent to having the x_{1i} and x_{2j} variables in our equations represent $h(x_{ab})$[1] where h is the Heaviside extractor activation function. In order to keep our mathematical notation as simple as possible, we will let it be understood that this clipping action is always implied in every calculation.

We can compactly write the mathematical description for R$^{(1)}$ in vector-matrix notation as

$$\begin{aligned}\mathbf{x}_1(t+\Delta t) &= \mathbf{x}_1(t) + \Delta t\cdot\left(-(\mathbf{A}_1 + \mathbf{F}_1 + \boldsymbol{\xi}_1)\otimes\mathbf{x}_1 + B_1\cdot(\mathbf{f}_1 + \boldsymbol{\xi}_1) - D_1\cdot(\mathbf{F}_1 - \mathbf{f}_1)\right)\\ \mathbf{x}_2(t+\Delta t) &= \mathbf{x}_2(t) + \Delta t\cdot\left(-(\mathbf{A}_2 + \mathbf{F}_2 + \boldsymbol{\xi}_2)\otimes\mathbf{x}_2 + B_2\cdot(\mathbf{f}_2 + \boldsymbol{\xi}_2) - D_2\cdot(\mathbf{F}_2 - \mathbf{f}_2)\right)\end{aligned} \quad . \qquad (16.3)$$

Here it is understood that everything on the right-hand side is evaluated at time t. $\mathbf{A}_1$ and $\mathbf{A}_2$ are constant column vectors ($n\times1$ and $N\times1$, respectively) with elements A_1 and A_2. $\mathbf{F}_1$ and $\mathbf{F}_2$ are column vectors with elements $F_k = \sum f_k(x_{k,m})$, $k = 1$ or 2, $m = i$ or j, with the sum taken on m over all the excitation variables in that layer according to the definition of F introduced in chapter 15. f_1 and f_2 are the activation functions for v_1 and v_2, respectively. We will assume f_1 and f_2 are the same general function but with layer-specific parameters $g_{\max}$, $u^{(1)}$, $u^{(2)}$ as per figure 14.7B. Without loss of generality, we will use (14.23) for the activation function in all examples.

[1] $a = 1$ or 2, $b = i$ or j.

$\mathbf{f}_1$ and $\mathbf{f}_2$ denote column vectors with entries $f_1(x_{1i})$ and $f_2(x_{2j})$, respectively. The symbol $\otimes$ denotes term-by-term multiplication with vectors $\mathbf{x}_1$ or $\mathbf{x}_2$. The remaining scalar terms are as previously defined in chapter 15. The iteration step size Δt is constrained by (d14.19) for whichever layer gives the smallest bound. Equations (16.1) through (16.3) define the dynamical system for $R^{(1)}$ except, of course, for its adaptation dynamics.

The first thing we must note about (16.3) is that these two matrix difference equations are *coupled* to one another through (16.1) and (16.2). The overall system of equations is therefore different than the system of equations for $CL^{(1)}$ in chapter 15. The coupling is what makes $R^{(1)}$ a resonator. There has been no widely disseminated paper comparable to [GROS14] published, which means we do not possess a set of theorems, analogous to those in chapter 15, that set down the mathematical properties of $R^{(1)}$. It is true that we can expect this system to behave in many ways like the one we studied in chapter 15. For example, the layers of $R^{(1)}$ each have a quenching threshold, QT_1 and QT_2. However, it should come as no surprise that this system also has *different* behaviors not in evidence in $CE^{(1)}$. We will encounter some of these later on in the examples presented here. The reason most of the theorems presented in chapter 15 cannot be assumed for $R^{(1)}$ is that the equation for $R^{(1)}$ is not the same as the equation for $CE^{(1)}$. Therefore we are not in possession of proofs of these theorems for the case of $R^{(1)}$. For this we would need a "new GROS14" – a formidable undertaking. Nonetheless, in a great many cases we will be able to use our knowledge of the Grossberg theorems to understand a number of important behaviors this system exhibits.

The general theme describing $R^{(1)}$ behavior is this. A vector of input signals is applied to v_1 and causes excitation of the x_{1i} variables. This is called an ***activity pattern*** – essentially just $\mathbf{x}_1$ – and constitutes the "short term memory" STM_1 of v_1. STM signals are projected to v_2 via $\mathbf{W}$ and set up an activity pattern $\mathbf{x}_2$. Feedback from the v_2 activity pattern to v_1 alters $\mathbf{x}_1$, which causes an alteration in $\mathbf{x}_2$, etc. A ***resonance*** is said to occur when both $\mathbf{x}_1$ and $\mathbf{x}_2$ settle into steady state fixed point solutions in response to the original applied inputs $\{ I_i \}$. When this input changes the system undergoes another transient leading to another fixed point resonance. Our main task in this chapter is to gain an understanding of this resonance process.

The desired state of affairs for the resonances of $R^{(1)}$ has two main features. First, it is desired that STM_1 be a representation – typically with some amount of contrast enhancement – of the input vector to v_1. The STM_1 vector, $\mathbf{x}_1 = \mathbf{\Theta}$, is the basis for the adaptation of $\mathbf{W}$ and $\mathbf{Z}$. Second, the activity pattern $STM_2 = \mathbf{x}_2$ is desired to represent an ***encoding*** of the original input signal vector. The *row* vectors W_j^T constitute the classifying vectors for $R^{(1)}$. The *column* vectors Z_i constitute a set of ***expectation vectors***. These vectors are said to "learn the patterns" $\mathbf{\Theta}$. To the extent that the **Θ** vectors represent the inputs { I_i }, v_2 is said to have ***categorized*** the inputs.

This explains *what* occurs. *How* does this work in $R^{(1)}$? The qualitative explanation is as follows. Let $\mathbf{I}_1$ and $\mathbf{I}_2$ be two external input patterns to v_1. Let us further suppose that both signals have previously been successfully coded by v_2 such that $\mathbf{I}_1$ is encoded by a 0-1 distribution in v_2 in which node x_{21} is the only active node. Similarly let $\mathbf{I}_2$ be encoded by a 0-1 distribution in which x_{22} is the active node. When $\mathbf{I}_1$ is presented to v_1, v_1 responds by generating an activity pattern STM_1 that excites v_2. By our assumptions, this will produce an excitation only in node x_{21}. This, in turn, generates a feedback vector $\mathbf{K}_1 = \gamma \cdot Z_1 \cdot h_2(x_{21})$. *In the ideal case* $\mathbf{K}_1$ will equal $\mathbf{I}_1$ except for a multiplicative factor determined by γ. v_1 now has a new input that is exactly the same as $\mathbf{I}_1$ except for a multiplicative factor. Thus, v_2 continues to receive an input signal that is the same, except for the multiplicative factor, that it received when $\mathbf{I}_1$ was first applied. This maintains the STM_2 pattern, the feedback to v_1, and thereby the system settles into a steady-state fixed point of operation. (This steady-state condition is what allowed W_1 and Z_1 to adapt to, ideally, a contrast-enhanced prototype of $\mathbf{I}_1$).

Now suppose the input changes from $\mathbf{I}_1$ to $\mathbf{I}_2$. The total input to v_1 is now $\mathbf{I}_2 + \mathbf{K}_1$, which, again ideally, will equal $\mathbf{I}_2 + c\mathbf{I}_1$, where c is the aforementioned scaling factor. This changes the activity pattern of STM_1 and the two inputs will compete, with $\mathbf{I}_2$ attempting to establish its unique activity pattern and $\mathbf{K}_1$ attempting to maintain the pattern associated with $\mathbf{I}_1$. If $\mathbf{I}_1$ and $\mathbf{I}_2$ are sufficiently different and if $\mathbf{K}_1$ is a sufficiently weaker signal than $\mathbf{I}_2$, the STM_1 activity pattern will change. In the extreme case, if $\mathbf{I}_2 + \mathbf{K}_1$ produces a *uniform* net input signal vector, then STM_1 will be abolished altogether. This is because the D_1 term in the $SNI^{(3)}$ equation produces an effect similar to the C term in $GN^{(2)}$. We recall that $GN^{(2)}$ suppresses uniform input patterns and produces a zero-vector output. The v_1 layer does the same. Thus, if $\mathbf{I}_2 + \mathbf{K}_1$ is uniform, STM_1 vanishes and, lacking an input excitation, v_2 also resets to the zero condition. But this removes the feedback signal $\mathbf{K}_1$ and so now v_1 "sees" only $\mathbf{I}_2$ and responds by producing the STM_1 pattern associated with $\mathbf{I}_2$. This reactivates v_2, this time producing the x_{22} 0-1 distribution. v_2 then feeds back $\mathbf{K}_2$ – which again is ideally just a scaled version of $\mathbf{I}_2$ – and the system "locks into" its new steady-state.

What happens if $\mathbf{I}_1$ and $\mathbf{I}_2$ are sufficiently different – which means they contain different *features* $R^{(1)}$ is using for its classification coding – but $\mathbf{I}_2 + \mathbf{K}_1$ does not produce a *uniform* input pattern? In this case, and again assuming $\mathbf{K}_1$ is a weaker signal than $\mathbf{I}_2$, the change in STM_1 will cause x_{21} to decrease (it is no longer seeing as strong an input signal) and cause x_{22} to increase (it is now "seeing" a stronger input because STM_1 contains the influence of $\mathbf{I}_2$). v_2 will begin to reverberate ***and if its quenching threshold is sufficiently high*** its activity pattern will be erased and replaced by the activity pattern for $\mathbf{I}_2$, much as we saw for $CL^{(2)}$ in chapter 15. Reverberation in v_2 at first weakens and then quenches $\mathbf{K}_1$ and replaces it with $\mathbf{K}_2$, the feedback vector for x_{21}.

This is the basic idea behind the operation of $R^{(1)}$. To achieve it: (1) the feedback signals must be weaker than the external input signals from $GN^{(2)}$; (2) v_1 must have a sufficiently high QT that new patterns erase and overwrite old STM_1 patterns; and (3) v_2 must likewise have a sufficiently high QT so that its STM does not persist when the input that caused it is removed. Whether or not $\mathbf{I}_1$ and $\mathbf{I}_2$ are "sufficiently different" depends on these vectors containing different *distinguishing features* that have been encoded into W_1 and W_2 (and into Z_1 and Z_2 which, ideally, are equal to W_1 and W_2, respectively, except perhaps for a constant scale factor). These are the Grossberg conditions for successful encoding and classification in $R^{(1)}$.

It will not have escaped your attention that the word "ideally" appears several times in the description just given. In practice, things are rarely ideal and this is the case for $R^{(1)}$. We have just ignored the details of the temporal dynamics that lead to all these changes in STM, and we have further invoked the still-vague notion $\mathbf{I}_1$ and $\mathbf{I}_2$ are "sufficiently different." We must meet and confront the nasty realities that lurk within the practical system and see how these nasty realities affect the ideal case we have just described. We will do this in the next section through the vehicle of a specific example system.

§ 3. Resonator 1 Dynamics with Binary-valued Input Patterns

It will suffice without loss of generality to study the dynamics of $R^{(1)}$ for a specific case. In this section we will study an $R^{(1)}$ network with $n = 25$ nodes in $GN^{(2)}$ and v_1, and $N = 3$ nodes in v_2. The parameters of the system will initially be set at:

- $GN^{(2)}$: $B_0 = 1$; $A_0 = 0.5$; $C_0 = B_0/(n-1)$
- v_1: $B_1 = 1$; $A_1 = 0.5$; $D_1 = 1.5$; $g_{\max 1} = 1$; $u_1^{(1)} = 0.85$; $u_1^{(2)} = 0.98$
- v_2: $B_2 = 1$; $A_2 = 0.5$; $D_2 = 1.0$; $g_{\max 2} = 1$; $u_2^{(1)} = 0.95$; $u_2^{(2)} = 0.98$

The feedback gain γ will be set to 0.05. These parameters were chosen empirically to yield an $R^{(1)}$ network with good performance and reasonable robustness in the simulation cases studied. For the sake of simplicity, we will consider the LTM weights in $\mathbf{W}$ and $\mathbf{Z}$ to be fixed. Thus the simulations are considered to take place after the system's adaptation process has established the classifying vectors. Adaptation will be considered in chapter 17.

Although all input signals are column vectors, as an aid to visualization we will present them as if they were arranged in a 5×5 square grid (a "retina") as we did in chapter 15. Figure 16.2 illustrates four representative input patterns, which we shall call T, J, X, and O, respectively. The weight vectors W_1 and Z_1 equal the T pattern except for scaling so that $|W_1| = |Z_1| = 1$. Similarly, W_2 and Z_2 are set to the J pattern, and W_3 and Z_3 are set to the X pattern.

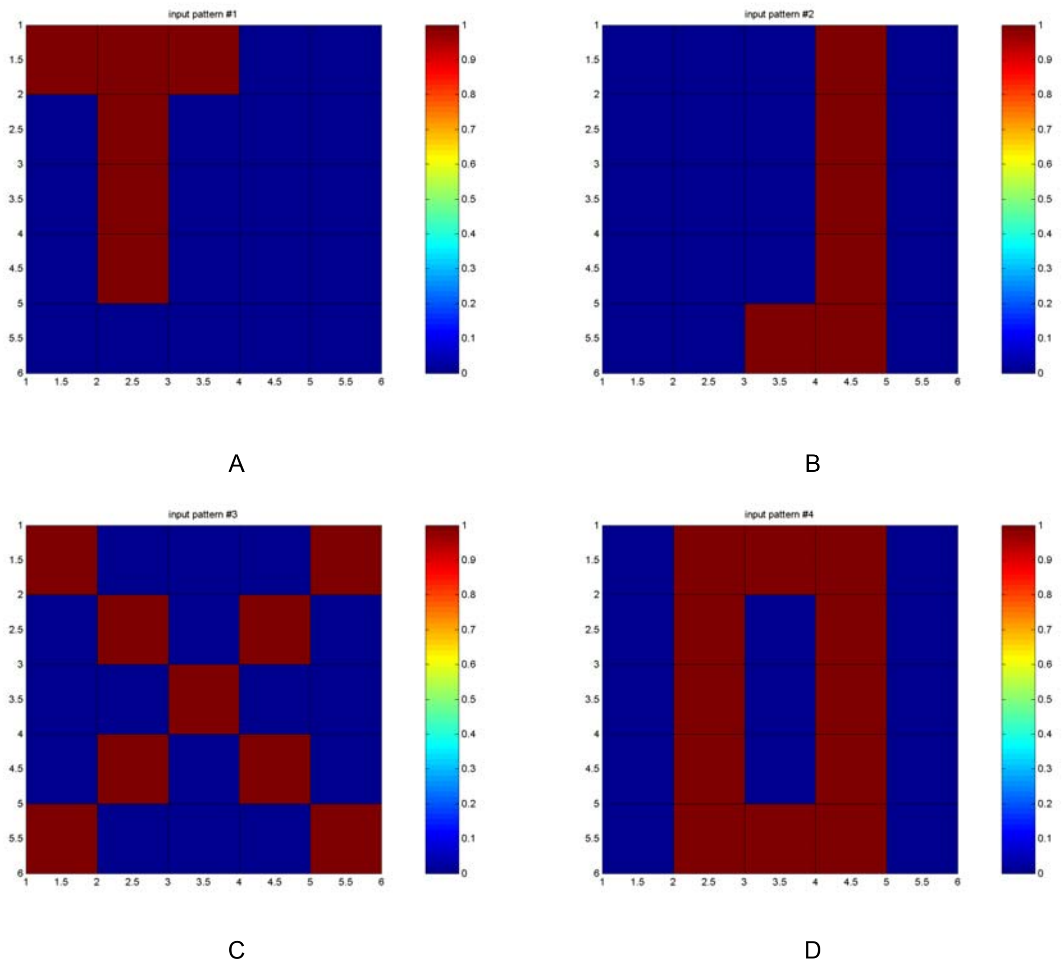

Figure 16.2: Representative input patterns for the example R$^{(1)}$ system. (A) pattern T. (B) pattern J. (C) pattern X. (D) pattern O. The LTM weights of the system are set equal in direction to the T, J, and X patterns and the weight vectors are scaled to unit length.

Where two retina patterns share common "pixels" the patterns are said to have *common features*. If we compare the T and J patterns, we see that these two patterns do not intersect at any pixel. T and J are said to be "well separated" or "completely distinct" from one another. The X and O patterns, on the other hand, each have non-empty intersects with the other three patterns, i.e. they both share common features with the other three patterns.

Finally, we must define the h_2 activation function in (16.1). For this we will begin with a rather poor choice, the popular Heaviside step function, i.e. $h_2(x) = 1$ if $x > 0$ and $h_2(x) = 0$ otherwise. We will soon see the compelling reason for changing this choice to the Heaviside extractor. This completes our parameter definition of the example R$^{(1)}$ system for now.

We will find it useful to have a way to measure and assess how closely the activity pattern $\mathbf{x}_1$ matches the input pattern $\mathbf{I}$ presented to v_1 by GN$^{(2)}$. In mathematics such a measuring function is called a ***metric function*** and the measure itself is called a ***distance***. Mathematicians have defined

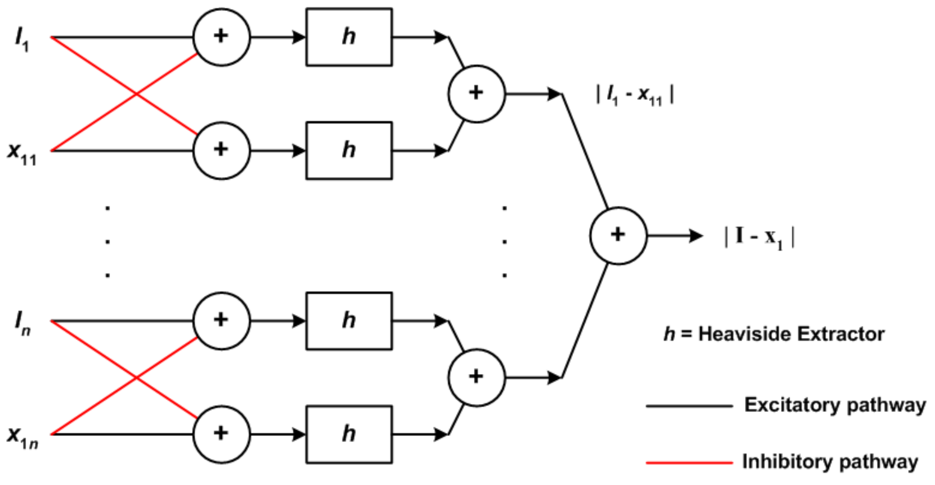

Figure 16.3: A biologically plausible Instar neural network system capable of implementing the absolute value metric function. The Instars in this network are conventional Instars, not SNIs.

many different kinds of distance metrics, the most familiar of which is the Euclidean distance metric. Our purposes here – namely the study of biological signal processing – are best served if our distance metric function is one that a neural network system can produce. In general, a function ρ is a metric function if it has the following three properties:

- For any pair x and y, $\rho(x, y) = 0$ implies $x = y$;
- $\rho(x, y) \geq 0$ for any pair x and y;
- For any x, y, and z, $\rho(x, y) + \rho(y, z) \geq \rho(x, z)$.

If **I** and **x** are vectors with n elements, the absolute value metric

$$\rho(\mathbf{I}, \mathbf{x}) = |I_1 - x_1| + |I_2 - x_2| + \ldots + |I_n - x_n| = |\mathbf{I} - \mathbf{x}|$$

is a valid metric function. It is easily verified that the simple Instar network of figure 16.3 generates this metric function, and so we will use the absolute value metric as our biologically plausible measure of the "distance" between **I** and $\mathbf{x}_1$.

Under the simplest form of adaptation – the IAR managed locally by $R^{(1)}$ – success depends on v_2 developing a 0-1 distribution at its outputs. Although we are not yet considering adaptation dynamics, the parameters of the system have been chosen to produce this type of coding. With N nodes in v_2, $R^{(1)}$ can classify at most N distinct categories. We will begin our examination by seeing how $R^{(1)}$ performs this task given weight settings that are exact copies of the T, J, and X patterns, and how it responds to the unclassified pattern O. As we will be applying patterns in a sequence of T → J → X → O, our first simulation series will be called the TJXO series.

TJXO1. Let the TJXO pattern sequence be corrupted by uniformly distributed random noise over a range (0, 0.02) relative to unit pixel amplitudes in the pattern. The noisy signal passes through $GN^{(2)}$ and the normalized input is applied to v_1. Figure 16. 4 shows the excitation, v_2, and

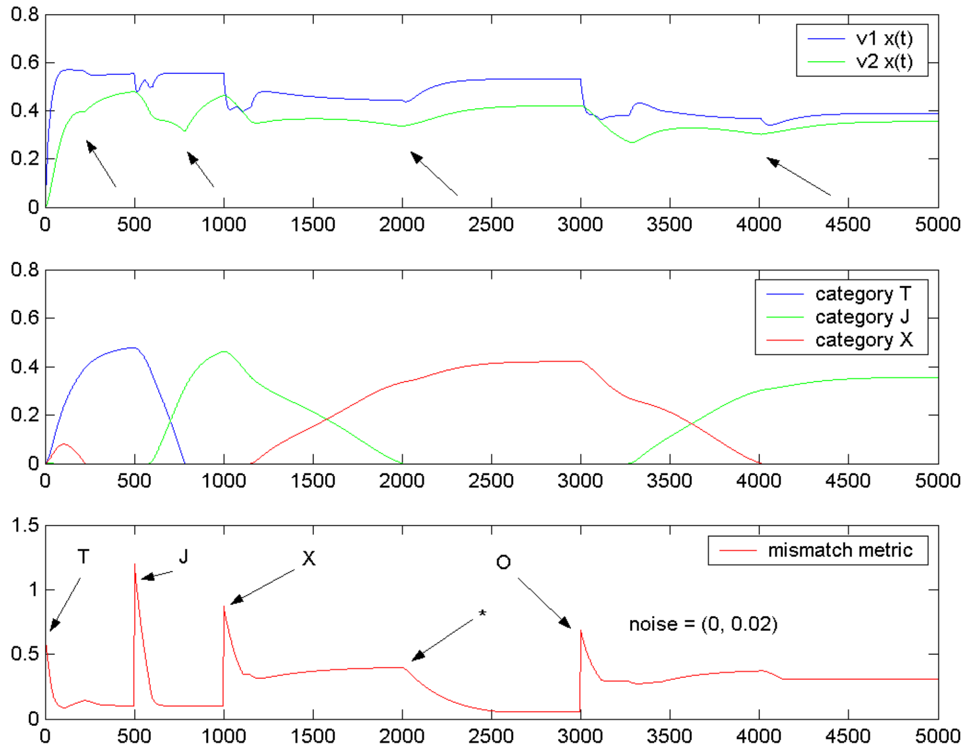

Figure 16.4: Response of R$^{(1)}$ to the TJXO sequence with upper noise bound of 0.02. The patterns were applied at the iteration steps indicated by the T, J, X, and O arrows in the mismatch metric trace. The total input pattern, including noise, was held constant through the duration of its application period.

the absolute value mismatch metric. The first thing we note is T and J were correctly classified quickly, and the low mismatch value attained indicates the pattern in v_1 was well matched to the input patterns **I** in both cases. Some degree of mismatch is to be expected because v_1 will quench the low-valued noise pixels and transfer their excitations into the pattern pixels. We may also note that the transition from T to J input is quite obvious from the spike in the mismatch at time index 500. We may also note from the top traces of the total excitations $x(t)$ that v_1 rather quickly settled into a stable distribution, but that v_2's response is considerably slower and had not leveled off by the time the transitions from T to J and from J to X took place.

Next we note that although X was eventually classified correctly with a low amount of $\mathbf{x}_1$ mismatch, it took much longer for R$^{(1)}$ to reach its decision. x_{22} ("J") and x_{23} ("X") competed for about 1000 iteration steps before x_{23} finally won out. It took over three times as long to settle this competition as it did for the system to switch from T to J. Not until time step 2000 did x_{23} take over definitive classification of the X pattern. Recall that X shares two common features (pixels) with the predecessor pattern J. The classifier had difficulty in "deciding" if it was "seeing" pattern

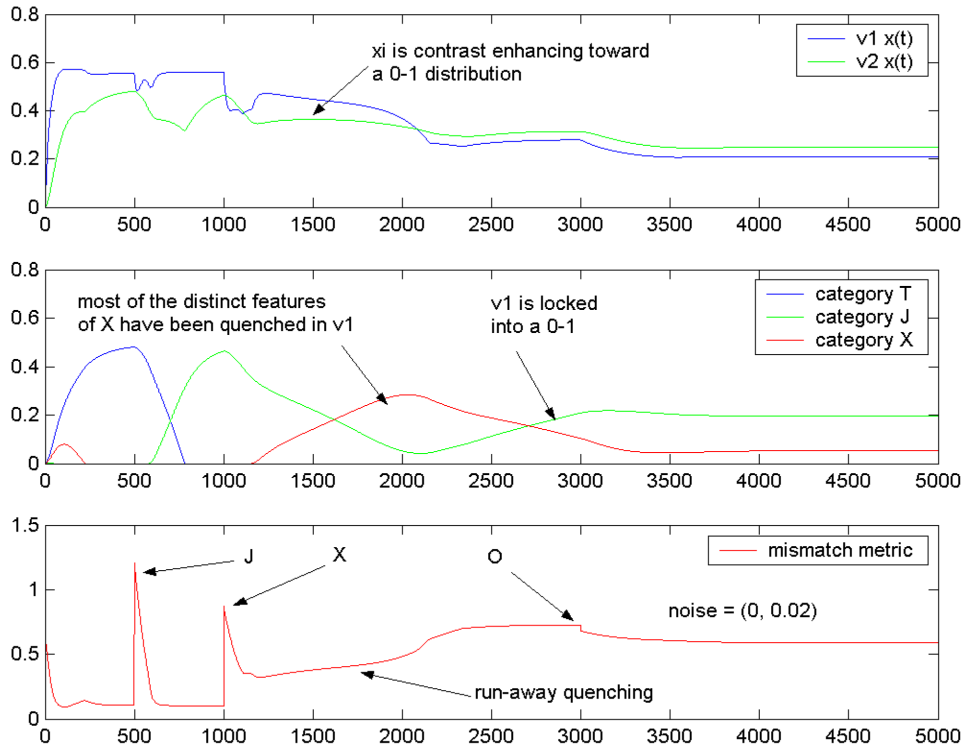

Figure 16.5: Replication of the first TJXO simulation with different noise patterns. Only the specific noise patterns varied in this run. $R^{(1)}$ fails to correctly classify the X pattern.

J or pattern X. One might suspect that this "longer, harder" competition is a symptom of lack of robustness to extraneous noise, and as we will see in a moment, this suspicion is justified. Finally, we note that $R^{(1)}$ could not decide on pattern O with both x_{22} and x_{23} active. In this case, layer v_1 locked into a 0-1 final distribution with the "surviving" v_1 pixel being a common feature of both J and X.

Figure 16.5 shows the results of repeating the first simulation with new random noise values. The previous suspicion about lack of robustness is confirmed in this run. $R^{(1)}$ fails to classify the X pattern in this run. The cause of the failure was run-away quenching of the X pattern by v_1 over the course of the competition. What survived in the v_1 pattern was again a pixel common to both J and X. This is our first look at a performance property of $R^{(1)}$ that will assume some significant importance, namely the effect of contrast enhancing and quenching v_1 will perform on its input pattern. Figure 16.6 illustrates the v_1 STM at iteration indices 2000 (when category "J" begins to overtake category "X") and 2999 (just before O is applied). Figure 16.6A clearly shows the severe amount of contrast enhancement that has taken place at step 2000. The X pattern is still faintly visible, but the two dominant pixels are features in common with J. The near erasure of the

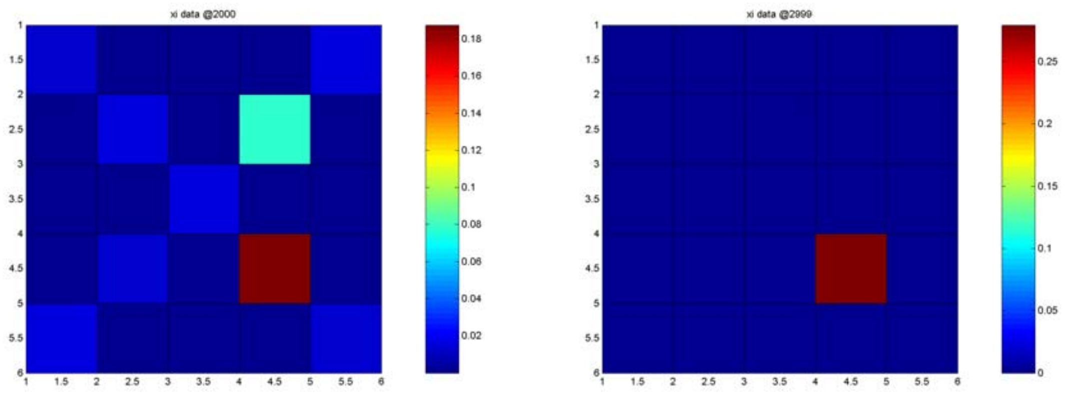

A B

Figure 16.6: v_1 STM pattern at iteration steps 2000 and 2999 for TJXO series number 2.

majority of the X features at time step 2000 (A) – which is what is meant here by the phrase "run-away quenching," – will become a total erasure by time step 2999 (B) except for the lone remaining dominant pixel.

Why did category J win out over category X in this simulation despite the X-pattern silhouette in 16.6(A) and the $x_{23} > x_{22}$ state at step 2000? There are two things to consider here. First, our use of the Heaviside step function for h_2 negates any amplitude advantage one x_{2j} node might have over another. With the Heaviside step function activation, activation is all-or-nothing. So far as the feedback to v_1 is concerned, **K** is as much determined by x_{23} as it is by x_{22}. The second thing to consider is what was said earlier about uniform or uniform-like inputs to v_1 reducing its STM. With the Heaviside step function h_2, the total feedback-plus-input is "more uniform-like" than either X or J alone would be. We can observe from the top trace of figure 16.5 that $x(t)$ for v_1 is constantly on the decline all during the x_{22}-x_{23} competition. Now recall also the theorems from chapter 15. As the lesser pixels decline in their X_i normalized amplitudes, the largest pixel will increase in its X_i amplitude. This appears to be the basic mechanism behind the excessive contrast enhancement dynamic in figures 16.5 and 16.6. The Heaviside step function is a poor choice for h_2 and leaves the system open to undue influence by very small amounts of pattern noise.

Replacing the Heaviside step function for h_2 with the Heaviside extractor, which you will recall preserves amplitude information for $x > 0$, makes a difference that may seem utterly out of proportion. Figure 5.7 illustrates a repeat of sequence TJXO under the same conditions except for the activation function h_2. Pattern X is easily and quickly classified by $R^{(1)}$. The decision dynamics are robust and x_{22} (category "J") is driven to zero by the stronger "X" feedback signal. Figure 16.8 illustrates the STM patterns in v_1 at the end of the J-pattern application period and in the middle of the X-pattern application period. No excessive contrast enhancement occurs.

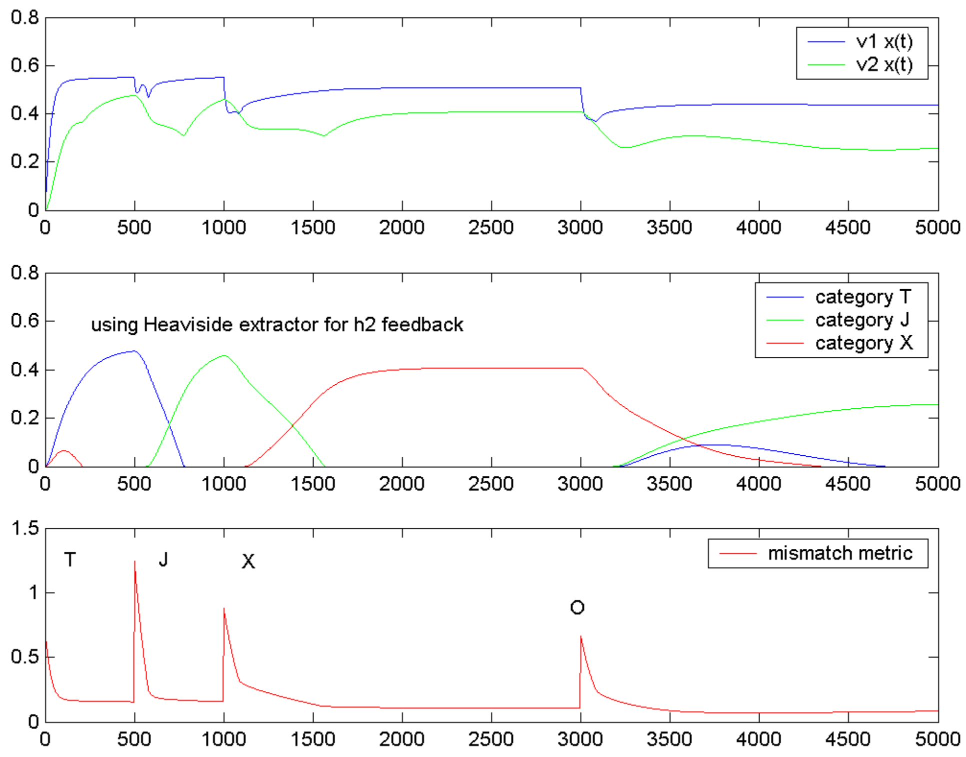

Figure 16.7: Replication of sequence TJXO using the Heaviside extractor function for *h*$_2$, noise = (0, 0.02).

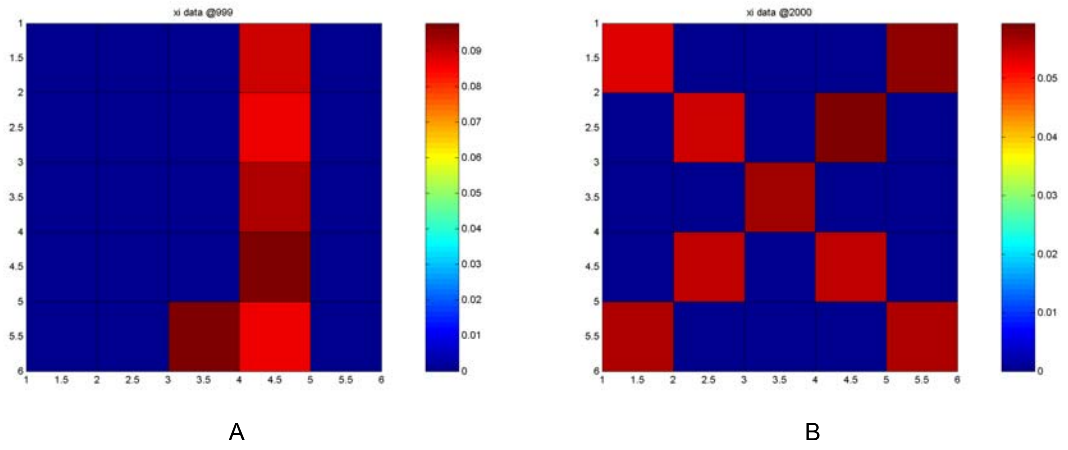

Figure 16.8: v_1 STM patterns just prior to pattern X application and at iteration step 2000.

As for pattern O, it is eventually classified as a "J" pattern. Interestingly, though, the residual STM in v_1 is a diminished O pattern roughly two-thirds the amplitude of 16.8B's pattern and about half as much as 16.8A. This is why the mismatch metric at time index 5000 in figure 16.7 is so small. O shares more common features with J than with either other classifying vector, and this is why v_2 classifies it as a J.

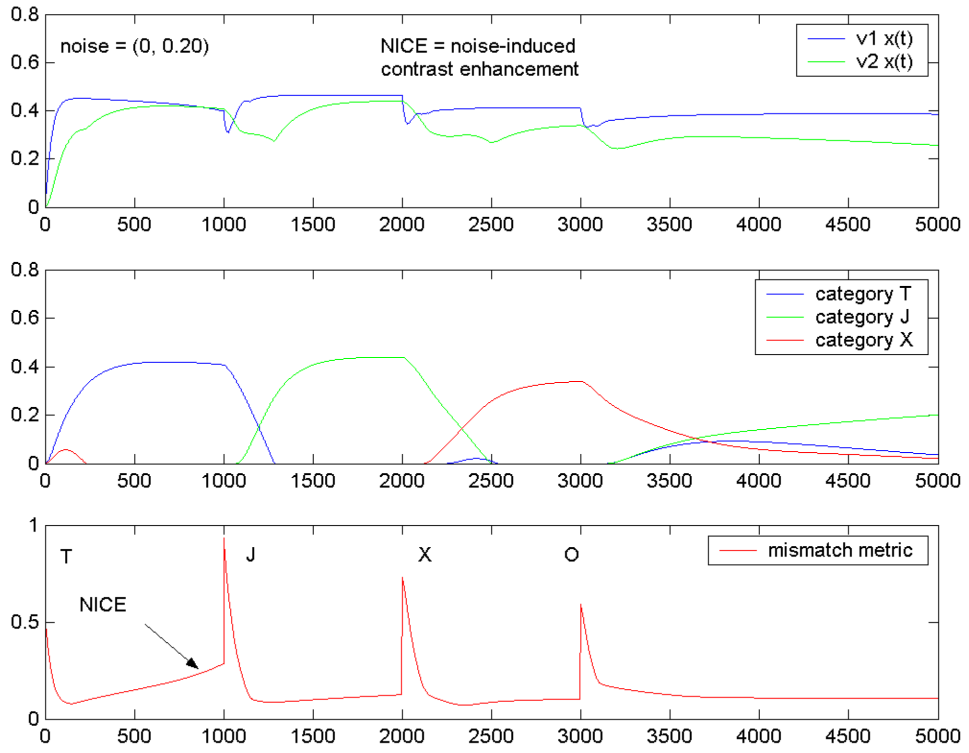

Figure 16.9: Noise-induced contrast enhancement (NICE) in a TJXO sequence.

There is another nonlinear noise effect present in $R^{(1)}$. The previous examples have all been run at relatively modest noise levels, uniformly distributed in the range (0, 0.02). At higher noise levels it is readily observed that pattern noise exerts an effect on the formation of STM in v_1. This effect is called ***noise-induced contrast enhancement*** or NICE. Despite the acronym, it is not a "nice" effect. We recall that IAR processing in its simplest form is fundamentally aimed at driving the classifying vectors to equal their prototype pattern models. When excessive amounts of contrast enhancement occur in v_1, this contrast enhancement will lead to a distortion of the classifying vectors.

The effect is exhibited modestly in figure 16.9 and more graphically in figure 16.10. The noise level for this simulation was set to the range (0, 0.20), a factor of 10 increase in the range of the pattern noise. Indications of NICE are seen in figure 16.9 in the droop in $x(t)$ for v_1 in the first 1000 iteration steps, and even more clearly in the rise of the mismatch metric in this same interval. The effect is shown explicitly in the STM_1 plots of figures 16.10.

Because NICE is a nonlinear noise effect, there is a great deal of variability in the extent of the effect when the system operates in a NICE region. Figures 16.11 and 16.12 illustrate the effect at

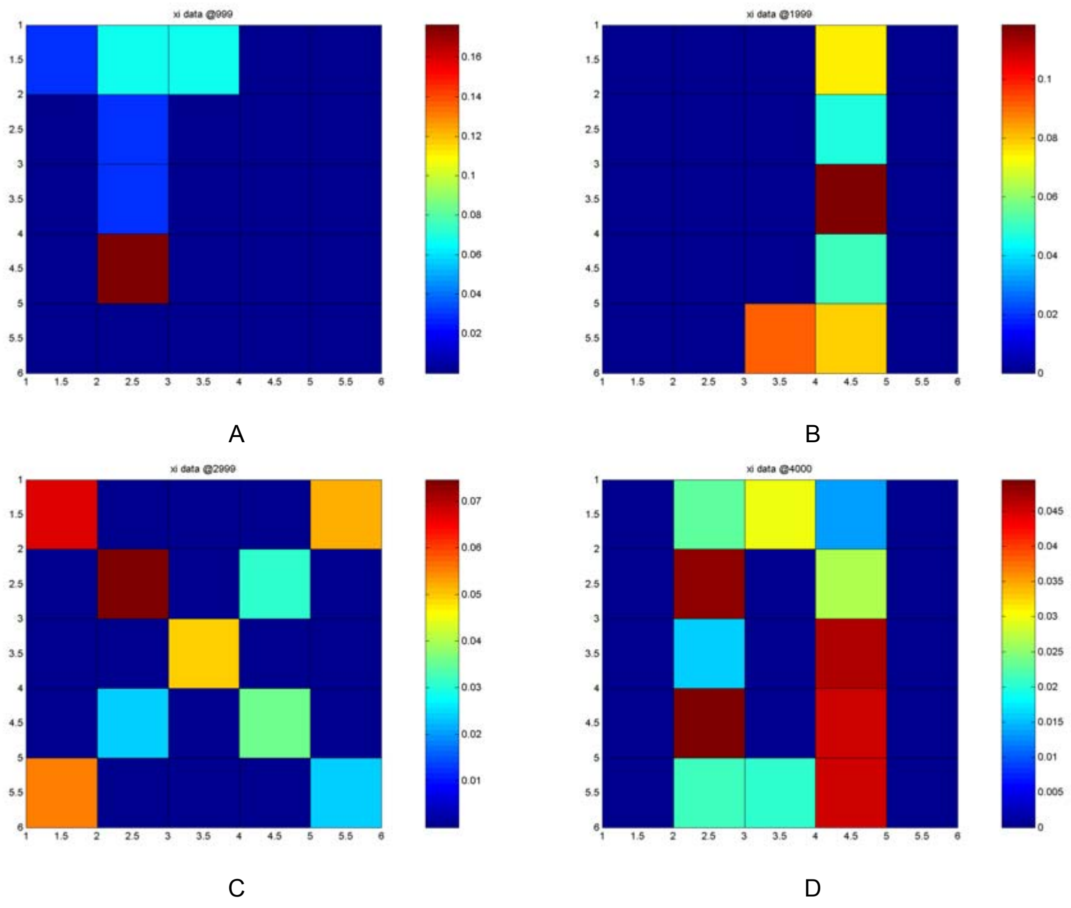

Figure 16.10: STM$_1$ showing extent of contrast enhancement for each pattern. (A) T-pattern at step 999. (B) J-pattern at step 1999. (C) X-pattern at step 2999. (D) O-pattern at step 4000.

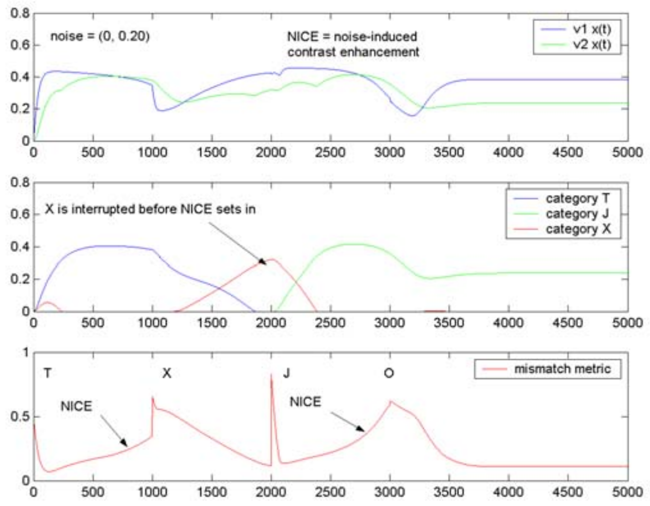

Figure 16.11: NICE effect in a TXJO pattern sequence. Note the sharp rise in mismatch metrics for the T and J patterns as well as the corresponding droops in $x(t)$ for v$_1$.

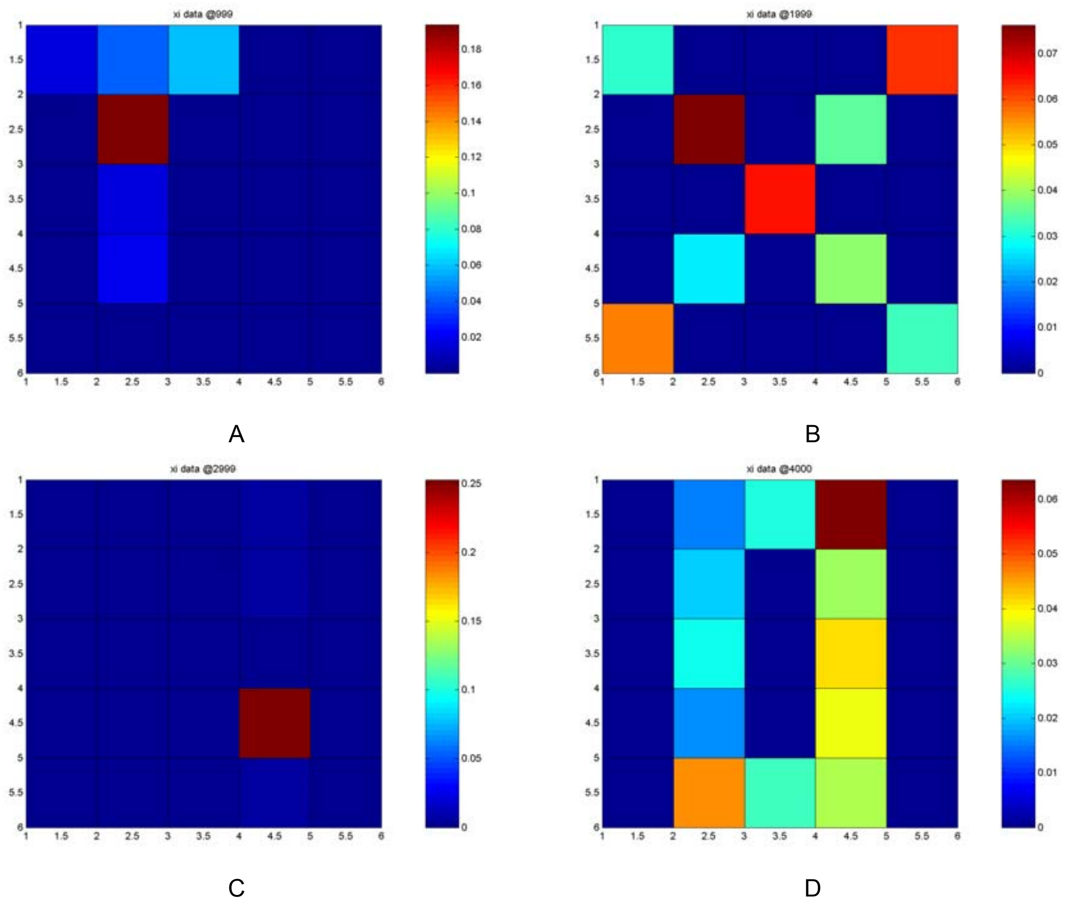

Figure 16.12: NICE STM patterns corresponding to figure 16.11. (A) J-pattern. (B) X-pattern. (C) J-pattern. (D) O-pattern. These STMs are sample just prior to the next pattern application except for the O-pattern.

the same noise levels for a TXJO pattern. Note especially in figure 16.11 how NICE during the T pattern interferes with the subsequent processing of the X pattern, and how pronounced the NICE curve becomes for the J pattern. The corresponding STM plots for each pattern are shown in figures 16.12. These may be compared with their pattern-counterparts in figures 16.10.

For noise uniformly distributed from 0 to r the expected value of the noise in each pixel is $r/2$ and the mean-squared value per pixel is $r^2/3$. Thus, the average pattern noise power is $nr^2/3$. The signal power is the sum of the squares of the pixel amplitudes, which is 6 for the T and J patterns and 9 for the X pattern. For $r = 0.20$, this corresponds to a ***signal to noise ratio*** (SNR) arriving at the input of $\text{GN}^{(2)}$ of 12.55 dB for T and J, and 14.3 dB for X. In contrast, for $r = 0.02$ the signal to noise ratios are 22.6 dB and 24.2 dB, respectively. Lower SNR implicates a greater spread in the X_i values being processed in v_1. We recall from Grossberg's theorems in chapter 15 that whether the response of a contrast enhancer will result in a fair distribution or a contrast enhancing distribution depends on the initial spread of X_i values and the quenching threshold factor $\text{QT}_1 = u_1^{(1)}/(B_1 - A_1/g_{\max 1})$. Raising QT_1 therefore will combat the onset of NICE.

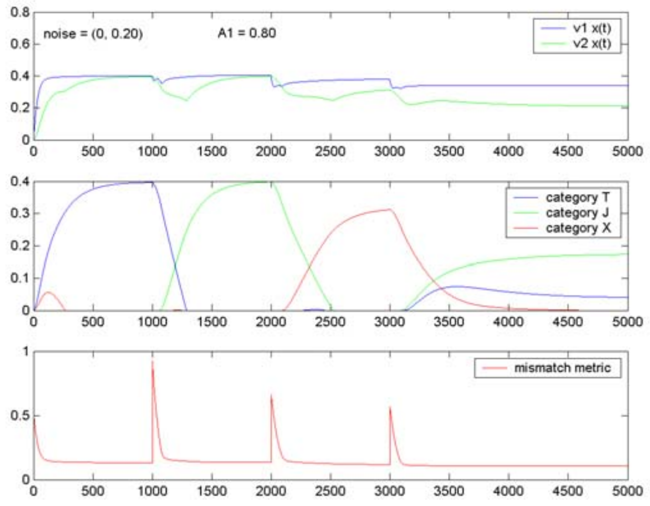

Figure 16.13: Effect of raising QT_1 on NICE effect for TJXO pattern sequence.

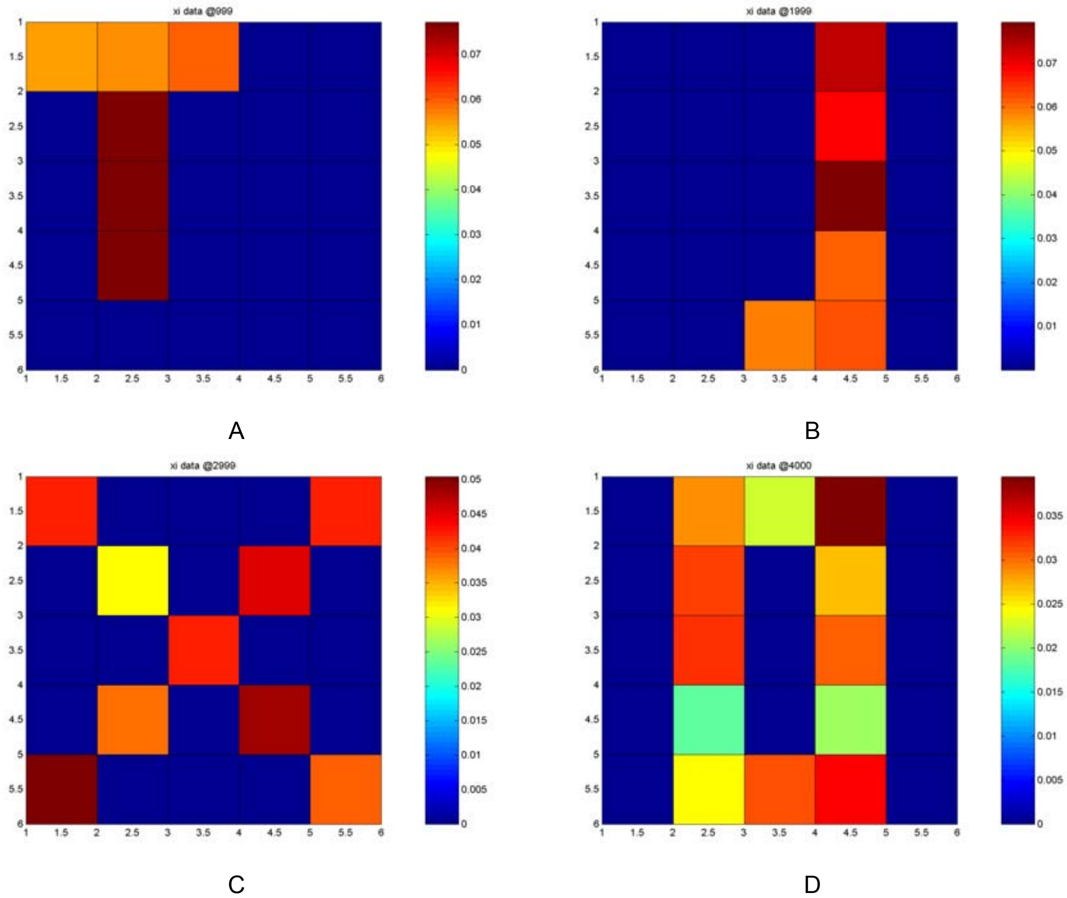

Figure 16.14: STM patterns corresponding to figure 16.13 achieved by increasing QT_1.

Figures 16.13 and 16.14 illustrate the effect of raising QT_1 by increasing A_1 from our base value of 0.5 to a new value of 0.8. $u_1^{(1)}$ remains at 0.85. The effect is a dramatic decrease in NICE for the noise distribution range (0, 0.20). Compare these results against figures 16.9 and 16.10.

To summarize where we are so far, we have seen that the choice of feedback activation function h_2 exerts an important effect on the dynamics of the system. We have compared the Heaviside step function against the Heaviside extractor and found the latter to be preferable in $R^{(1)}$. We have seen that the competition between v_2 nodes in establishing a resonance benefits from allowing the amplitude information in v_2 to act as a selection mechanism. We have examined the performance of $R^{(1)}$ as a classifier at high SNR levels and seen that it performs this task quite well. Finally, we have examined the nonlinear phenomenon of noise-induced contrast enhancement, found this to be a serious impairment at low SNR levels, and seen that the effect is combated by increasing QT_1. In our specific example, this was done by raising A_1 to $0.8B_1$ from our starting value of $0.5B_1$. We henceforth adopt these changes in our example system.

Feedback Gain. Up to this point, we have said nothing about the feedback gain factor γ. This parameter plays an important role in determining the dynamics of the system. For instance, in all our previous examples we have observed v_2 to produce 0-1 distributions for patterns corresponding to its classification vectors. However, the value for D_2 is $D_2 = B_2$, a level which in chapter 15 produced only a contrast-enhanced fair distribution and not a 0-1 distribution in $CL^{(2)}$ (see figure 14.22A). This difference between $R^{(1)}$ and $CL^{(2)}$ is caused by the feedback.

The feedback gain must be large enough so that, in conjunction with the magnitude of the weight settings z_{ji}, it supports persistence in STM_1 in the presence of an unchanging input pattern $\mathbf{I}_1$ but, at the same time, promotes decay in STM_1 when a new input $\mathbf{I}_2$ arrives that "belongs" to a different classifying vector W_j. If γ is too small, it will fail to promote resonance in $R^{(1)}$. But if it is too large, it will prevent $R^{(1)}$ from properly responding to new inputs and instead push it into a "lockup" condition with the two STM patterns "stuck" on whatever initial input produced them. The effect is illustrated in figure 16.15 for a TJXO pattern with $\gamma = 0.50$, a tenfold increase over the example system's base value of 0.05. Observe that the system had difficulty in switching from the T-pattern input to the J-pattern input (two well-separated patterns), and that the system failed completely to switch from the J to the X when that pattern arrived. Observe how the X-weight node x_{23} never responded at all to the X input.

Fortunately, the range of values for γ is rather broad and its precise setting does not seem to be particularly critical for proper system operation. In the example system the pattern weights are of unit length, meaning, for example, that the non-zero z_{ji} weights for the T-vector are $1/(6)^{½} = 0.408$. Typical x_{2j} values appearing in the signal traces are about 0.4 peak, and so $\gamma = 0.05$ yields a per-pixel feedback signal amplitude of about 0.008. This compares to $\mathbf{I}_1$ per-pixel values on the order of about 0.04 after the pattern has passed through $GN^{(2)}$, a 5:1 ratio of input to feedback.

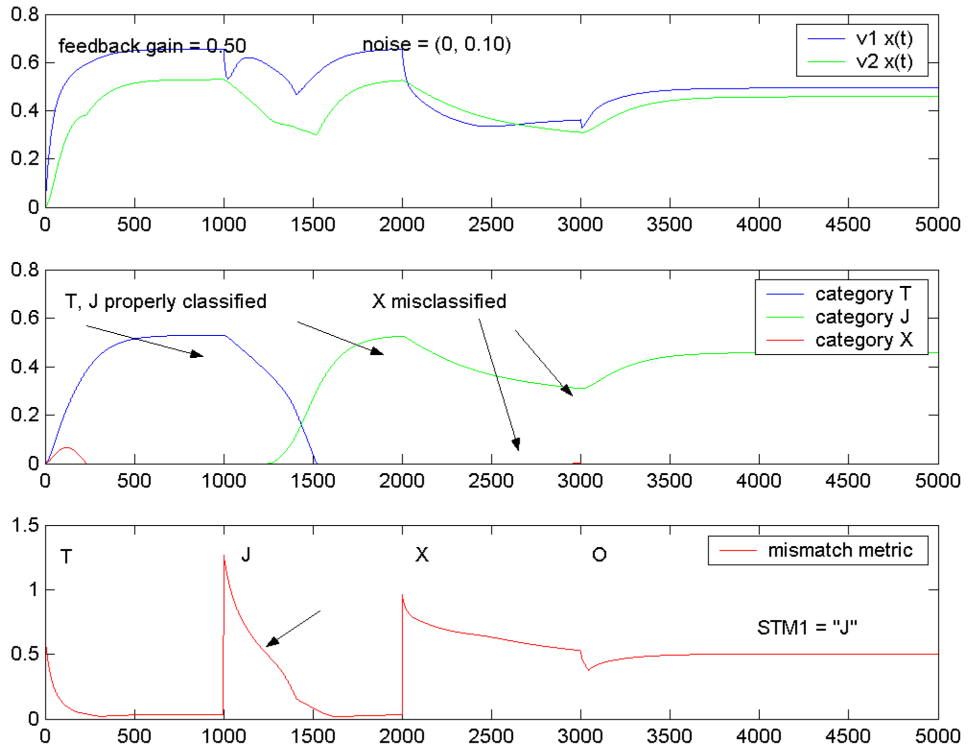

Figure 16.15: Effect of too-large feedback gain on R$^{(1)}$. Note the difficulty with which the system switched from the T to the J pattern, and its inability to recognize the X pattern. The O pattern was entirely overridden by the J-weight feedback, producing a J-pattern in STM in place of the O-pattern input.

§ 4. Resonator 1 Dynamics with Continuous-valued Input Patterns

Operating as a pattern categorizer with fixed weights and in the absence of noise, R$^{(1)}$ is remarkably robust to flat changes in pattern amplitudes, i.e. equal scaling of each pixel value. Figure 16.16 illustrates the example of a T-X-T-X pattern sequence in which the pattern amplitude of the T pattern is 1 and the pattern amplitudes of the two X patterns are 0.5 and 0.01, respectively. Both X patterns are successfully reproduced in v_1 STM (figures B and C) with a mere 4:1 amplitude difference (despite the fact that the X inputs going into GN$^{(2)}$ had a 50:1 difference). The first X pattern was successfully recognized by v_2. The smaller of the two X patterns was not successfully recognized (v_2 was mildly "bewildered" as shown in A) but the x_{23} ("X") signal did come out much stronger than the other two. Other than for an additional delay in the activation of x_{23} following the application of the X patterns, the resonance characteristics showed little pattern-to-pattern variation.

If one thinks about this a little, this is a fairly remarkable accomplishment for R$^{(1)}$. How did these things happen? There are several factors at work here. Let us begin with the actions of GN$^{(2)}$

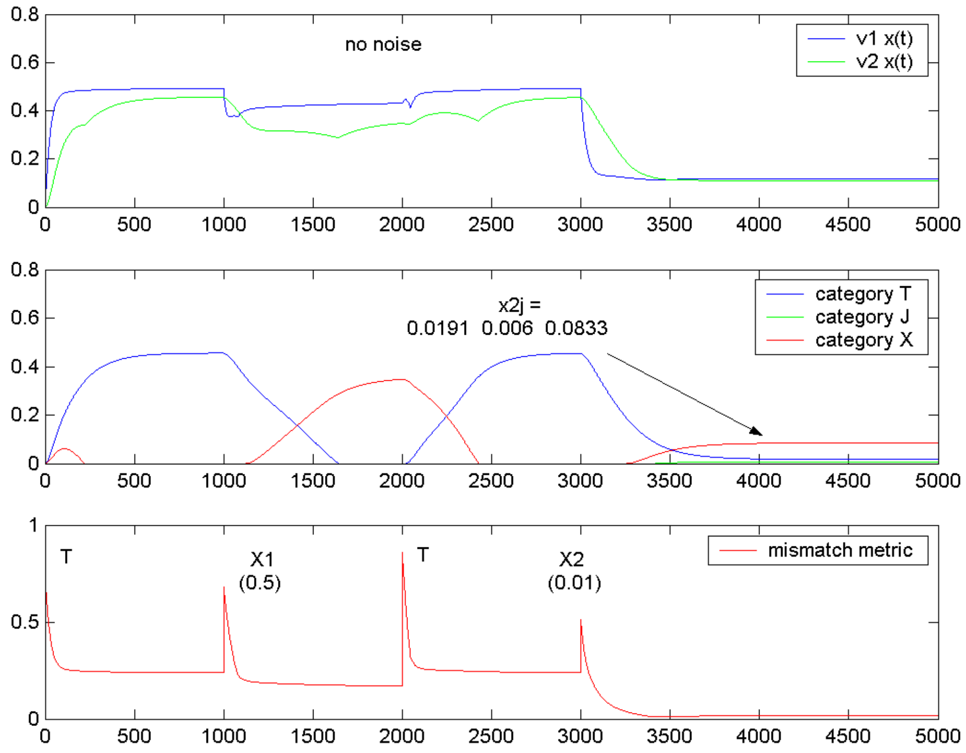

A

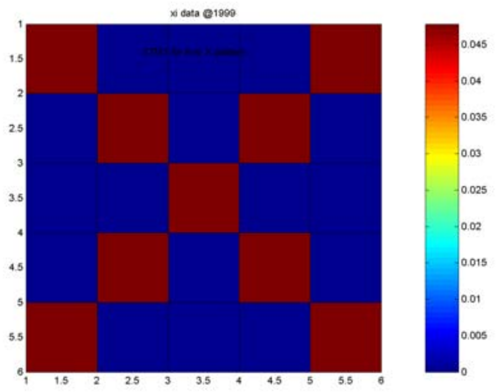

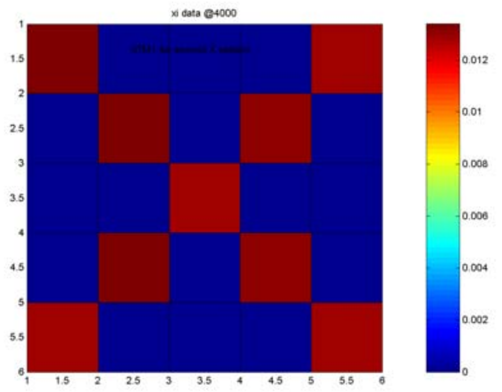

B

C

Figure 16.16: STM_1 patterns for X-pattern of amplitude 0.5 (B) and 0.01 (C). Signal traces are shown in (A). There is good reproduction of the STM, other than for an amplitude drop. The second X pattern was not cleanly encoded, as shown in (A), although x_{23} did have the largest amplitude of the x_{2j} variables. There was no pattern noise applied in this simulation. Note that although the two X pattern inputs differed in amplitude by a factor of 50:1 going into $GN^{(2)}$, the STM amplitude difference is only about 4:1.

normalization. Here we apply equation (14.12). If the non-zero pixel amplitudes have amplitude a then for the X pattern the total signal activity is $G = 9a$ (there are 9 non-zero pixels in X). For the non-zero pixels the relative amplitudes are $\omega_i = 1/9$. Using $B = (n - 1)C$, we rewrite (14.12) and obtain

$$x_i = \frac{n}{n-1} \cdot \frac{BG}{A+G}\left(\omega_i - \frac{1}{n}\right).$$

We have $B = 1$, $A = 0.5$, and $n = 25$ for our $GN^{(2)}$. For $a = 0.5$, this gives us $x_i = 0.0667$. For $a = 0.01$ we get $x_i = 0.0113$. What was a 50:1 amplitude ratio going into $GN^{(2)}$ is only a 5.9:1 ratio coming out. The Grossberg normalizer takes large amplitude spreads and compresses them into a much smaller range.

Next let us consider the absence of sequence interaction. Why did the STM set up by the large T pattern not overwhelm the smaller incoming X patterns? The reason is because of the quenching threshold dynamics of v_1. At the feedback level we are using, feedback from v_2 is not sufficient to sustain STM_1 when the input pattern changes significantly. Thus, STM_1 begins to decay, and it takes the x_{2j} values with it during its decline. Thus, with a Heaviside extractor activation function for the feedback, the feedback signals K_{ji} likewise fall. This is why the prior T activity could not block the smaller X activity from initiating a new STM. This can clearly be seen in figure 16.16A. It is true that the amount by which x_{21} must decay before x_{23} can "take over" is larger for larger amplitude differences between the T and X patterns. This is what causes the small increase in the time required for x_{23} to become active in 16.16A. But once it does, the resonance quickly develops and $R^{(1)}$ takes itself into the new X state in its STM patterns.

Next we note that the X pattern in STM_1 does not contrast-enhance. This is because the final distribution dynamics in a Grossberg CE layer (which is what v_1 is) do not depend on absolute individual signal amplitudes but, rather, on the normalized amplitudes $X_i = x_i/x$. This is why per-pixel signal amplitude does not affect the development of STM_1 in the absence of noise.

Why did v_2 fail to cleanly categorize the smaller X pattern? This is because the final v_2 distribution pattern *does* depend on *total* activity $x(t)$, which *is* smaller for the small X pattern. Instead of contrast-enhancing the pattern into a 0-1 distribution, the v_2 layer was only able to produce a partially contrast-enhanced output for its x_{2j} variables. We saw this same thing in some of the examples from chapter 15.

Unfortunately, this happy state of affairs does not maintain when pattern noise is present. If we make the usual assumption that pattern noise is statistically independent of the patterns, pattern noise does not drop in amplitude along with the input pattern. The result of this is, as you perhaps have already realized, noise-induced contrast enhancement (NICE) as a function of input pattern amplitude. We will call this amplitude-induced contrast enhancement or AICE.

Figure 16.17 illustrates AICE in a TXTX sequence. In this simulation the noise distribution is (0, 0.20), the T pattern has amplitude 1 in its non-zero elements, and the X pattern amplitudes are 0.5 and 0.1, respectively.

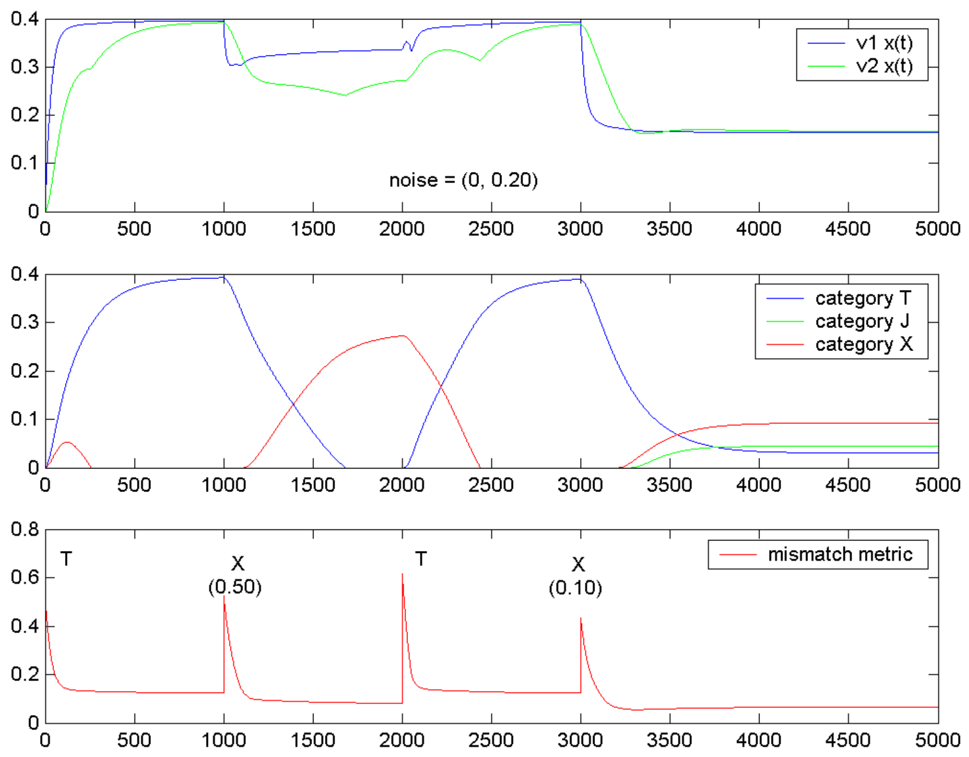

A

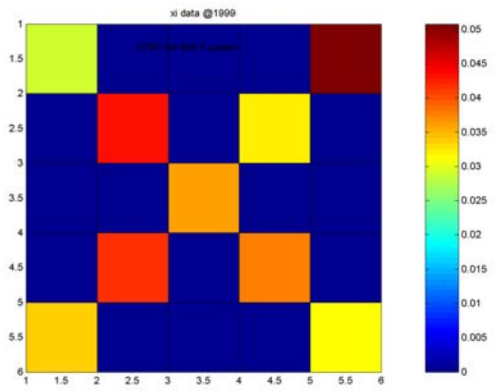

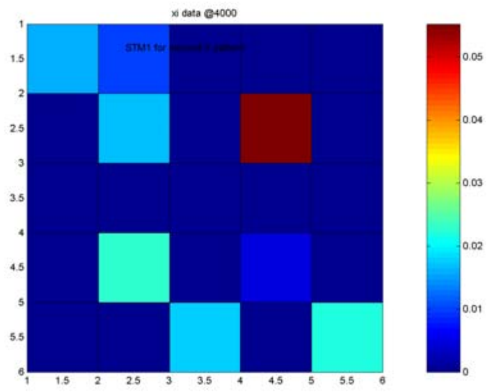

B C

Figure 16.17: TXTX sequence with pattern amplitude sensitive NICE (AICE). The T pattern amplitudes are 1.0. The X pattern amplitudes are 0.50 (B) and 0.10 (C). The pattern noise distribution is (0, 0.20). The contrast enhancement distortion in (B) is not severe enough to affect pattern categorization. The AICE in (C) produces a coding failure.

We have so far considered only input patterns with underlying pixel values of either 1 or 0, or patterns that are merely scaled versions of these. These kinds of patterns are typically called "binary" patterns because a pixel is either "on" or "off". It is true enough that contrast enhancement and additive noise produce continuous-valued pattern signals, but the terminology is

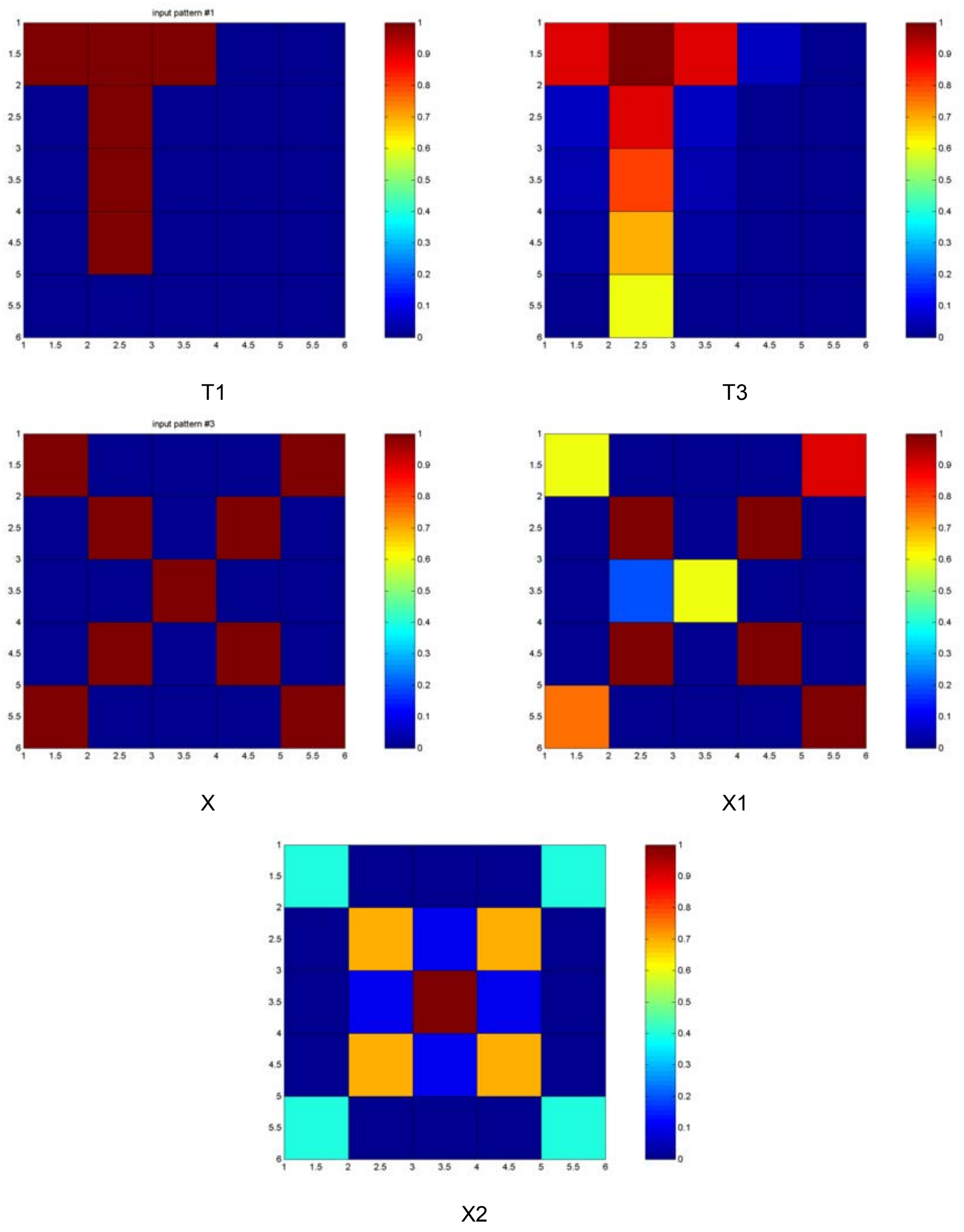

Figure 16.18: Analog pattern definitions. The label under each figure will be used to identify the pattern in the simulations. The new patterns are not contrast-enhanced. Their underlying pattern is defined as shown.

the same nonetheless. We now turn to consideration of patterns with continuous-valued underlying pixel definitions. These are commonly called "analog" patterns. Figure 16.18 illustrates several such patterns we will define and use in the next series of simulations. For ease of comparison, the figure sets these new "analog" patterns against their "binary counterparts" we have been using so far.

The significance in introducing analog patterns lies partly in the phenomenon of *fine discrimination* and partly in its opposite, generalization. As an example of the first, if you know a pair of "identical twins" it is possible and common after a short while to be able to tell one from the other by noting subtle differences that exist in their appearances, while other people, who do not know them, cannot tell them apart. Examples of the second are provided by any general class of identifications such as "man", "dog", "automobile", etc. These sorts of feature distinction and object assimilation are what analog patterns such as those above are used to model. Our next topic, then, is how $R^{(1)}$ performs when given subtly different yet distinct input patterns. As we are about to see, contrast enhancement effects (NICE and AICE) are important impairments in classifying analog patterns.

We will begin with generalization. In our first example $R^{(1)}$ is presented with a pattern sequence T3-X1-X2-T3 with the fourth pattern scaled to one-half the magnitude of the first. We assume moreover that no pattern noise is added. Figure 16.19 gives the trace results of the simulation. Despite the differences between these patterns and the baseline patterns stored in the weights **W** and **Z**, the system has no problem in properly classifying the patterns.

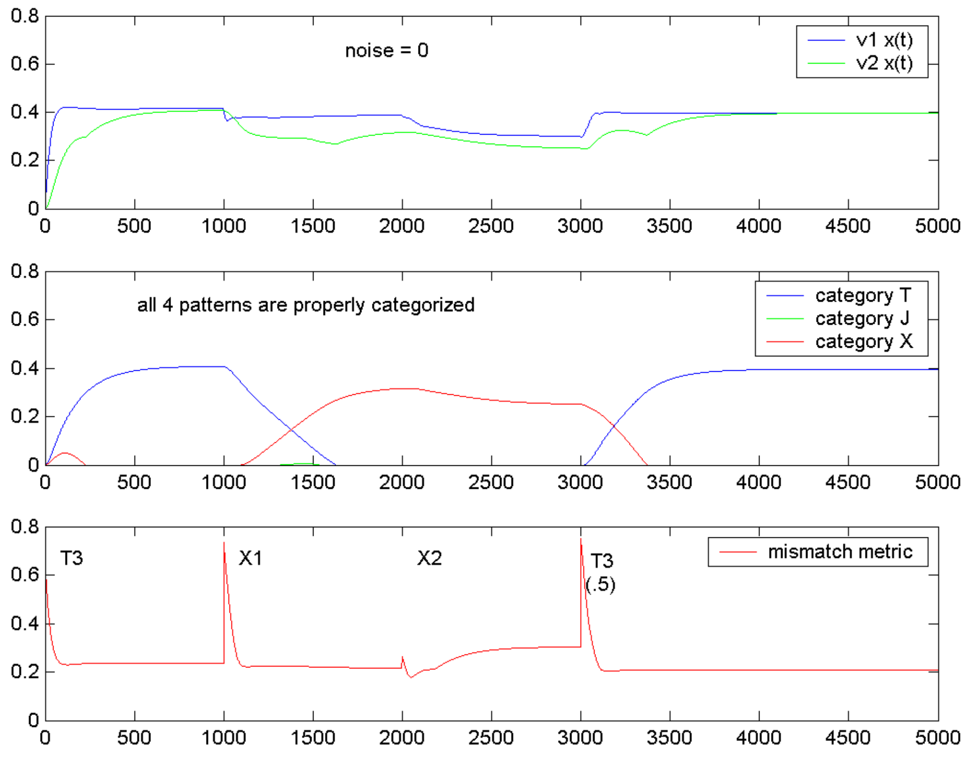

Figure 16.19: Simulation traces for T3-X1-X2-0.5T3 sequence. The system successfully classifies all four patterns.

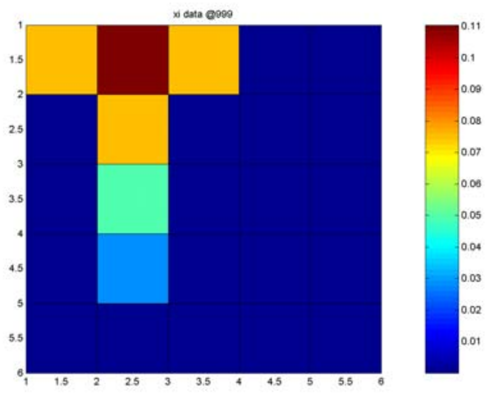

A

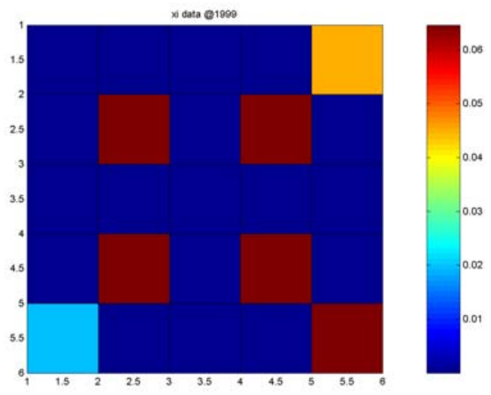

B

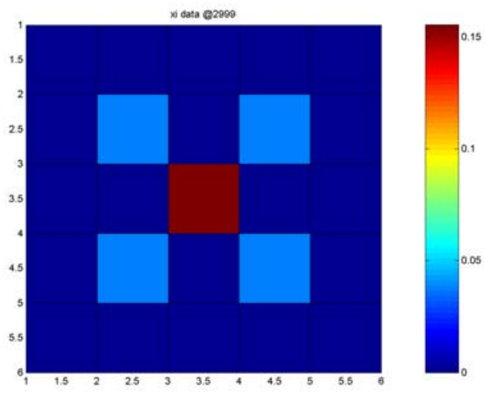

C

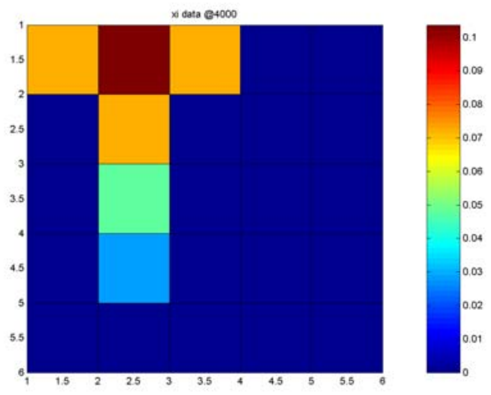

D

Figure 16.20: STM_1 patterns at time indices 999, 1999, 2999, and 4000 for the T3-X1-X2-0.5T3 simulation.

Now consider the patterns developed in STM during this simulation. These are illustrated in figure 16.20. Comparing these plots to the original patterns in figure 16.18, we see that significant contrast enhancement has been performed on the patterns. $R^{(1)}$ has thus not only generalized the patterns according to its classifying vectors, but has done so despite this contrast enhancement. This illustrates the ability of the network to *generalize*. But why has such radical contrast enhancement occurred?

The mechanism is, of course, the same as that which underlies NICE and AICE and is found in Grossberg's contour-enhancement theorems of chapter 15. Indeed, one interesting way to look at an analog pattern **A** is to regard it as a scaled version of the sum of a binary pattern **B** plus a noise pattern **N** such that $\mathbf{A} = s \cdot (\mathbf{B} + \mathbf{N})/|\mathbf{B}+\mathbf{N}|$ where s is some scale factor. By making **N** sufficiently large, "missing pixels" – pixels of level zero in **A** that are non-zero in **B** – can be approximated by letting **N** have a zero-value in that pixel location. From this way of looking at things, contrast enhancement of analog patterns can be viewed as another species of NICE.

Since $R^{(1)}$ successfully decoded the pattern in the example above, is this contrast enhancement

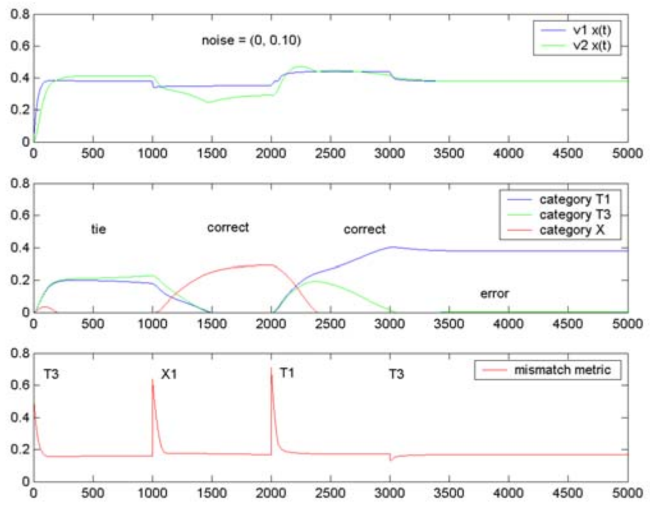

Figure 16.21: Simulation results for T3-X1-T1-T3 sequence with noise (0, 0.10). $R^{(1)}$ fails to discriminate between patterns T1 and T3 in the first and fourth locations.

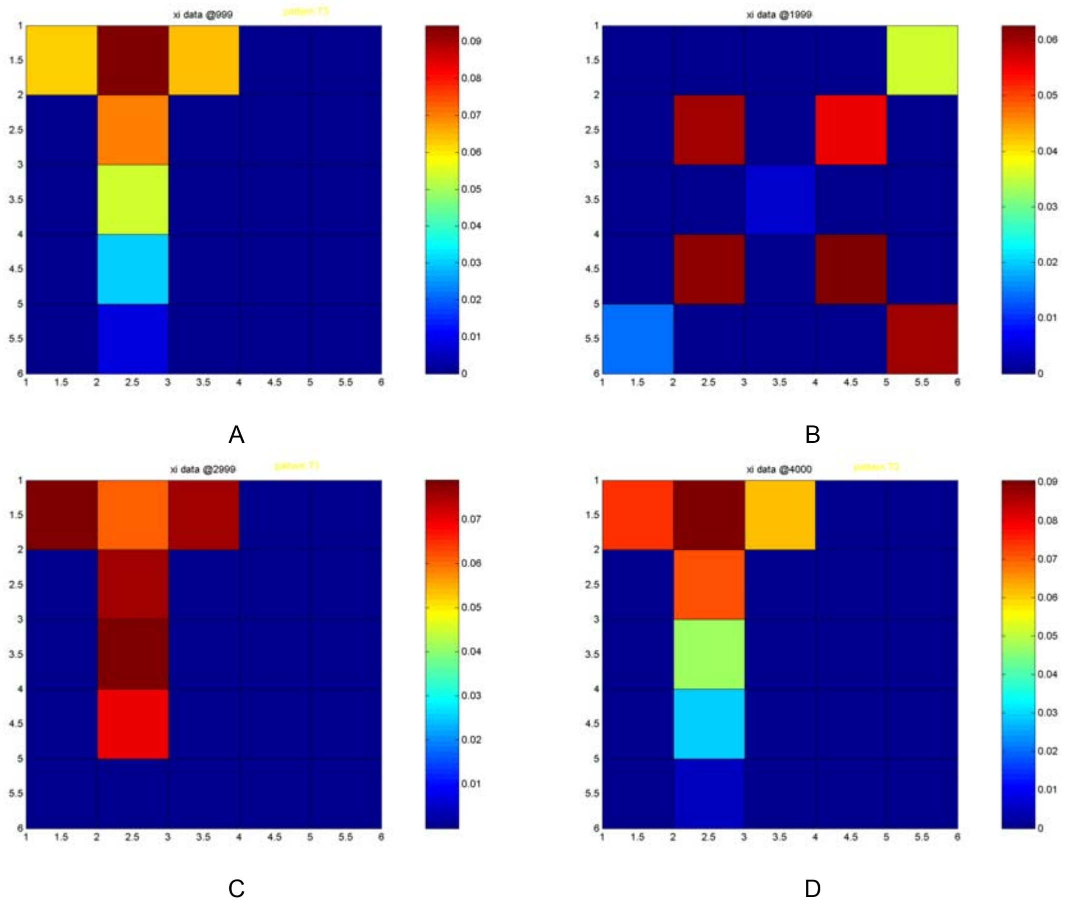

Figure 16.22: STM patterns for the T3-X1-T1-T3 pattern sequence simulation.

really a problem? The answer is "no" if we consider only the generalization problem, and "yes" when we come to the fine discrimination problem. Suppose we wish to discriminate between patterns T1 and T3, and to this end we replace the classifying vector for J in $R^{(1)}$ with a classifying vector T3. Figure 16.21 gives the results of simulating a sequence T3-X1-T1-T3 in the presence of additive pattern noise drawn from a uniform distribution over the range (0, 0.10), and figure 16.22 illustrates the STM patterns for the simulation.

$R^{(1)}$ is unable to categorize the initial T3 pattern, producing x_{21} and x_{22} activations of almost the same magnitude. Comparing 16.22A against the T patterns of figure 16.18, we see that the contrast-enhanced STM differs from both. In one sense it is a "blending" of both patterns, which is easy enough to understand from figure 16.21, where we see both classifying vectors contributing in nearly equal amounts to the feedback vector **K**. But the STM pattern is by no means merely the average of the two patterns; it has been contrast enhanced and not simply summed and scaled. The final result is, in a sense, as much like classifying vector T1 as it is for T3.

$R^{(1)}$ successfully classifies X1 – where its task in this case has been merely generalization – and it correctly classifies T1, which has undergone only relatively modest contrast enhancement due in part to the additive noise and in part to some initial feedback contributions from the T3 classifying vector (see figure 16.21). But it completely errs in classifying the final T3, mistaking it for a continuation of T1. Figure 16.21 shows that the T3 classifying vector is never even brought into play. The reason for this is easy to understand: the abolition of STM when inputs change is based on the new pattern producing a more uniformly distributed excitation of v_1. T1 and T3 are simply too much alike for the latter to abolish the STM left over from the former.

Would $R^{(1)}$ have performed better on this simulation if there had been no noise? The answer is, "no, it does not perform differently in any significant way." There are limits to what the basic ART resonator network can do by itself.

§ 5. Resonator 2

Historically, resonator 1 is the oldest of the published ART resonators. It is not, however, the only kind of ART resonator. In this section we will look at a simpler but still very effective ART resonator. We will call it ***resonator 2*** ($R^{(2)}$ for short).

In $R^{(1)}$ layer v_2 does make some modest contribution to contrast enhancement of STM_1, but the majority of NICE effects are due to the lateral feedback connections in v_1. This implies that NICE can be reduced if these connections are removed. $R^{(2)}$ does just that, replacing v_1 with a non-recurrent layer of the form

$$\dot{x}_{1i} = -A \cdot x_{1i} + \left(B - x_{1i}\right) \cdot J_i^{+} - \left(D + x_{1i}\right) \cdot J_i^{-} \qquad (16.4)$$

where we continue to use our convention that x_{1i} actually denotes $h(x_{1i})$, where h is the Heaviside extractor activation function. J_i^+ is the total excitatory input to node i and J_i^- is the total inhibitory input to node i. In the v_1 layer of $R^{(2)}$, neither of these terms contain any contribution from v_1 and so v_1 is, except for its Heaviside extractor activation function, a *linear* network for all x_{1i} with activity > 0. NICE is an inherently *nonlinear* effect, and this is why this new v_1 layer does not contribute to it. We will see that the remaining residual NICE contributed by v_2 is much smaller than the magnitude of the effect in $R^{(1)}$.

When the two J terms are zero, (16.4) tells us x_{1i} will undergo an exponential decay to zero at a rate determined by A. A is often called the ***neper frequency*** and its inverse is a ***time constant***, τ. With some simple algebraic manipulation, we can rewrite (16.4) as

$$\tau \cdot \dot{x}_{1i} = -x_{1i} + \tau \cdot (B - x_{1i}) \cdot J_i^+ - \tau \cdot (D + x_{1i}) \cdot J_i^- .$$

Now, if τ is very small, the transient response of this system will be much faster than that of the v_2 layer and v_1 will reach its forced response while v_2 is still reverberating. Setting the derivative equal to zero (the forced response condition if v_1 responds much faster than both v_2 and the input signal rate) and solving for x_{1i} we obtain

$$x_{1i} = \tau \cdot B \cdot \frac{J_i^+ - B_3 \cdot J_i^-}{1 + \tau \cdot J_i^+ + \tau \cdot J_i^-}, \quad B_3 = \frac{D}{B} . \tag{16.5}$$

We will use (16.5) as our model equation for v_1 in $R^{(2)}$. We will designate the Instars in this layer as $SNI^{(4)}$.

It still remains to define the two J signals. For J_i^+ we use (16.1) and obtain

$$J_i^+ = I_i + \gamma \cdot \sum_{j=1}^{N} z_{ji} \cdot h_2(x_{2j}) \tag{16.6}$$

which is the same excitation used by $R^{(1)}$. Here h_2 is the Heaviside extractor. For J_i^- we use

$$J_i^- = \sum_{j=1}^{N} h_2(x_{2j}) . \tag{16.7}$$

Expression (16.7) is called a ***non-specific activity*** in ART terminology. Its employment in (16.4,5) is called a ***non-specific inhibition*** [GROS6, 16], [CARP2]. In the anatomy of $R^{(2)}$, the term $B_3 \cdot J_i^-$ is also called an ***attentional gain control*** because it exerts an effect by which v_1 is influenced differently by input signals **I** than by v_2 excitatory feedback signals **K**. Replacing v_1 by the system defined by equations (16.5)-(16.7) gives us the system depicted in figure 16.23.

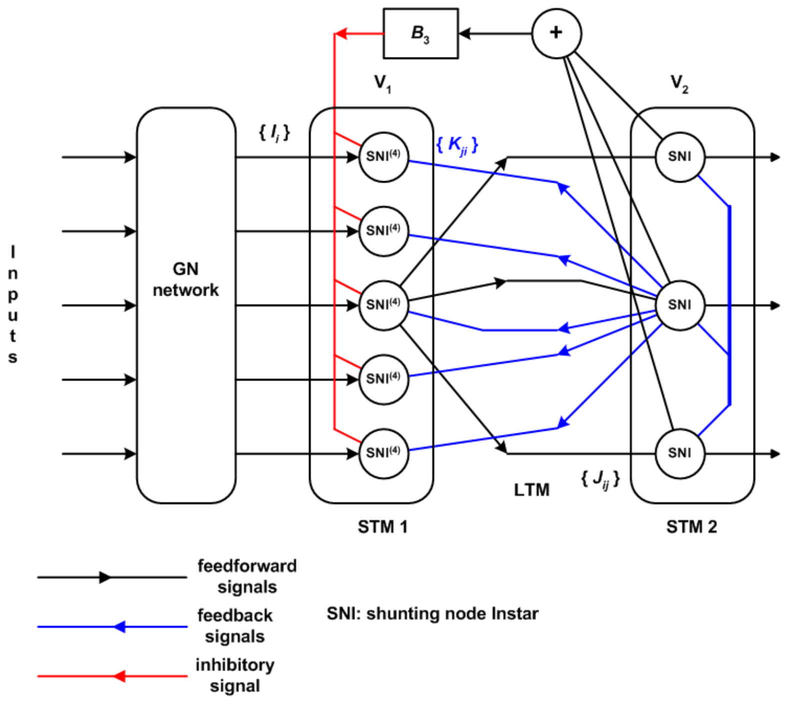

Figure 16.23: Resonator 2 system.

The behavior of this anatomy is illustrated in the following simulations. In these simulations we use GN$^{(2)}$ for the normalizer and the same v_2 layer as used for the R$^{(1)}$ simulations. The parameters for these subsystems remain unchanged from their previous values. For the v_1 layer the parameters are: (1) $\tau \cdot B = 1$; (2) $\tau = 0.001$; (3) $B_3 = \mu \cdot \gamma$ with $\mu = 0.5$ and γ (the feedback gain for $\mathbf{K}$ from v_2) equal to 0.05 as in R$^{(1)}$.

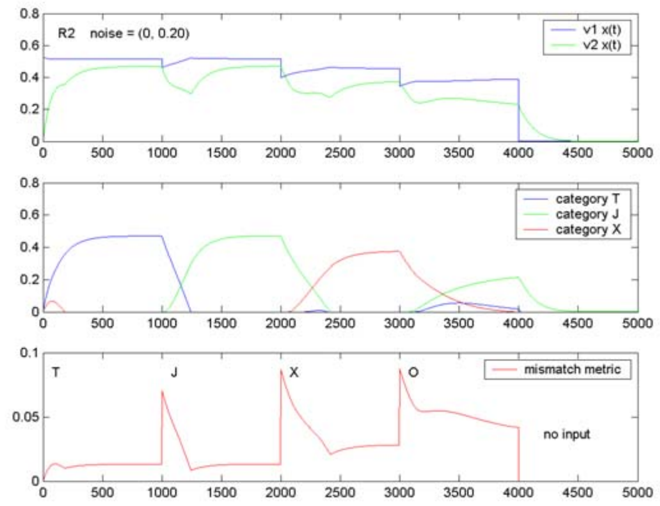

Figure 16.24: Standard TJXO sequence for R$^{(2)}$. The input parameters for this test sequence are the same as used previously in the first R$^{(1)}$ examples. All patterns have the same relative weighting. The additive pattern noise distribution is (0, 0.20). The network correctly classifies the T, J, and X patterns. There is very little NICE in STM$_1$. Pattern O is misclassified and its STM$_1$ is recognizably the O pattern.

The first simulation is a repeat of the TJXO series we first used to examine $R^{(1)}$. Figure 16.24 provides the signal traces for this simulation. Acting as a classifier, the performance of $R^{(2)}$ is equivalent to that of $R^{(1)}$ for the known patterns, and more or less the same for the unknown pattern O. The same continues to hold true for the other pattern tests used earlier. The differences between the two resonators shows up in STM_1. We may first note that although v_1 has a very fast response to signals (as it should), the total amount of time to process the incoming signals is not significantly different from that of $R^{(1)}$; layer v_2 dominates this aspect of the system dynamics. The biggest difference is the near-total lack of contrast enhancement distortion (NICE) in STM_1. Almost all the pattern distortion in STM_1 is directly due to the additive pattern noise itself, which is to be expected. This point will be demonstrated in the next simulation, where the performance advantage of $R^{(2)}$ in regard to NICE is more graphically illustrated. STM_1 plots are not presented for the present simulation because, quite frankly, they are boring. The T, the J, and the X come out looking like T, J, and X with all background noise squelched and only a small amount of additive noise visible in the pattern pixels. This is demonstrated by the mismatch metric in 16.24.

Our second simulation is a T3-X1-T1-J sequence (all patterns equally weighted) with pattern noise distribution (0, 0.20). This test is almost identical to the simulation of figure 16.22, with the use of the J pattern at the end being the only difference of consequence. Figure 16.25 shows the signal traces for this simulation, and figure 16.26 provides the STM_1 patterns.

Looking first at figure 16.25, we observe that all four patterns were properly classified by $R^{(2)}$. Like $R^{(1)}$, $R^{(2)}$ is incapable of distinguishing the alternative T and X patterns given weights that are exact copies of these patterns. The mismatch metric is significantly less than for $R^{(1)}$, which is

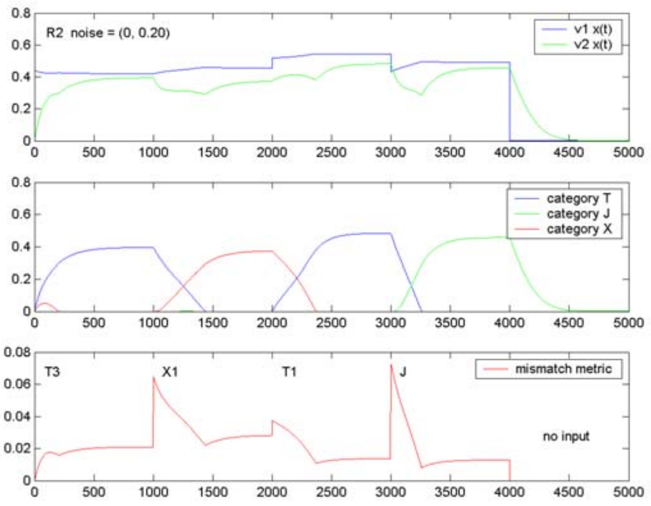

Figure 16.25: Signal traces for T3-X1-T1-J pattern sequence. $R^{(2)}$ correctly classifies all four patterns.

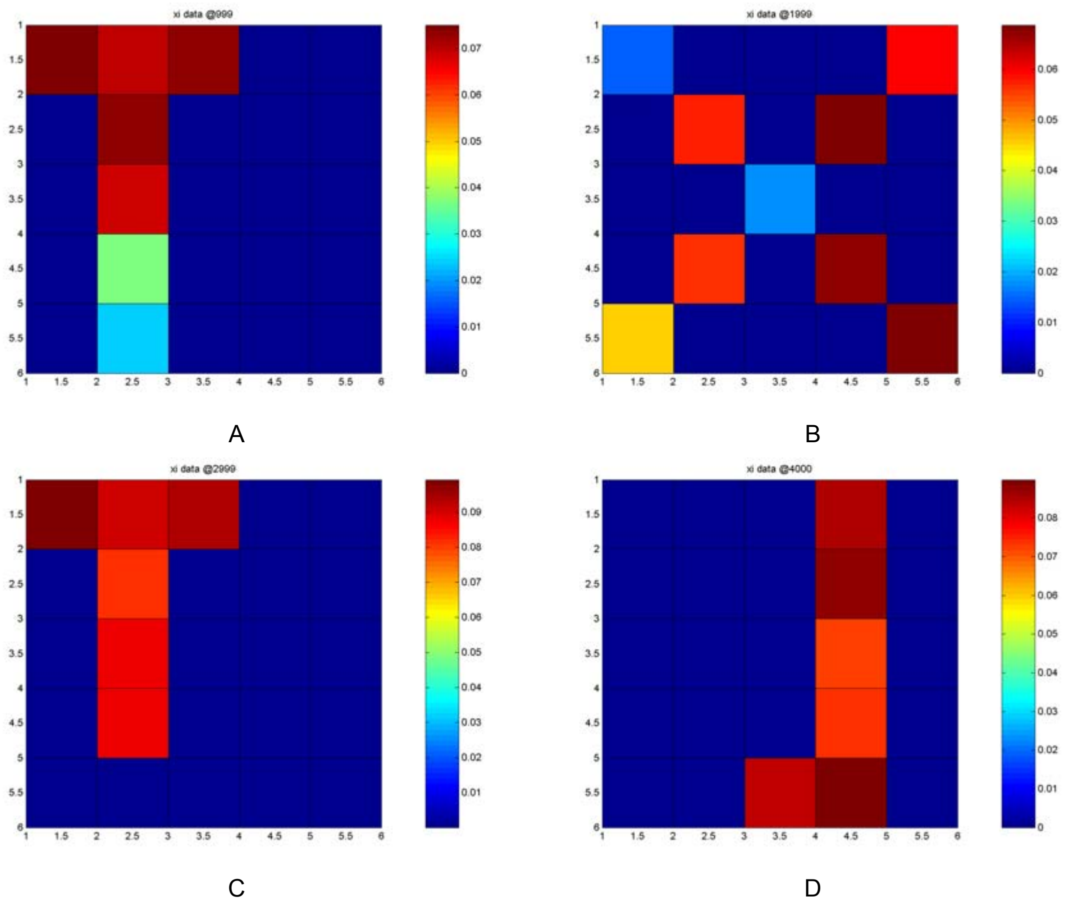

Figure 16.26: STM$_1$ plots for the T3-X1-T1-J sequence. Note that there is very little distortion of the STM patterns. Comparison of these patterns with figure 16.22 demonstrates that NICE is suppressed by R$^{(2)}$ leaving primarily additive pattern noise distortion only. Close examination of the numerical results of the simulation shows that some NICE does persist, but it is negligible compared to the additive pattern noise. Note also that the noise in this simulation is twice the amplitude of that used for figure 16.22.

a reflection of the absence of NICE effects in R$^{(2)}$. It is to be noted that the additive pattern noise distribution for this simulation is twice the amplitude of that used previously in the R$^{(1)}$ example simulation.

Next we examine figure 16.26. Comparing this figure to figure 16.22 from the R$^{(1)}$ simulation, we can easily see the dramatic improvement in preserving the input pattern in STM$_1$ realized by R$^{(2)}$. Again, this better copy-fidelity is despite the fact that twice as much pattern noise was added prior to GN$^{(2)}$. Other simulations, corresponding to figure 16.21, show that the failure of R$^{(2)}$ to be able to make the fine discrimination between, say, T3 and T1 is not due to the STM but, rather, to *the settings of the weights themselves*. As we will see in chapter 17, the fine discrimination problem is fundamentally a problem Carpenter and Grossberg call the ***subset-superset*** problem [CARP2]. Its solution is intimately tied in with the solution of the stability-plasticity issue in adaptive neural network systems. This is something we take up in chapter 17.

§ 6. Summary

This chapter has introduced two basic resonator networks of the sort commonly used in ART network system models. By themselves, these networks ***do not yet constitute a full ART system***. They are resonators, but we have not yet made them ***adaptive*** resonators. We will see in the next chapter that adaptation, methods to address fine discrimination, and the stability-plasticity problem require additions to the network system for controlling the adaptation process itself.

In this chapter we have given our attention to the basic resonance dynamics in play in minimal ART resonator networks. The theory presented here is largely comes from Grossberg's 1976 paper [GROS6], which preceded the first artificial ART network, ART 1 [CARP1], by almost a decade. As mentioned at the beginning of this chapter, our focus in this text is biological signal processing and computational neuroscience rather than engineering applications of ART. However, the material presented here should be of great help to those interested in engineering neural networks, and in helping to understand some of the thinking that goes into the classic ART papers of Carpenter and Grossberg.

Exercises

1. x